

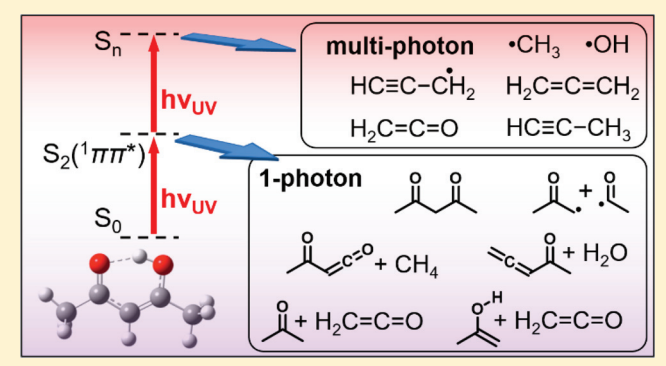
## To Boldly Look Where No One Has Looked Before: Identifying the **Primary Photoproducts of Acetylacetone**

Published as part of The Journal of Physical Chemistry virtual special issue "Hanna Reisler Festschrift".

Ivan Antonov, <sup>†</sup> Krisztina Voronova, <sup>‡,||</sup> Ming-Wei Chen, <sup>†,⊥</sup> Bálint Sztáray, <sup>‡</sup> Patrick Hemberger, <sup>§</sup> Andras Bodi, <sup>§</sup> David L. Osborn, <sup>†</sup> and Leonid Sheps\*, <sup>†</sup>

Supporting Information

ABSTRACT: We investigate the gas-phase photochemistry of the enolone tautomer of acetylacetone (pentane-2,4-dione) following  $S_2(\pi\pi^*) \leftarrow S_0$  excitation at  $\lambda = 266$  and 248 nm, using three complementary time-resolved spectroscopic methods. Contrary to earlier reports, which claimed to study one-photon excitation of acetylacetone and found OH and CH<sub>3</sub> as the only important gas-phase products, we detect 15 unique primary photoproducts and demonstrate that five of them, including OH and CH<sub>3</sub>, arise solely by multiphoton excitation. We assign the one-photon products to six photochemical channels and show that the most significant pathway is phototautomerization to the diketone form, which is likely an intermediate in several of the other product



channels. Furthermore, we measure the equilibrium constant of the tautomerization of the enolone to diketone on S<sub>0</sub> from 320 to 600 K and extract  $\Delta H = 4.1 \pm 0.3 \text{ kcal} \cdot \text{mol}^{-1}$  and  $\Delta S = 6.8 \pm 0.5 \text{ cal} \cdot \text{mol}^{-1} \cdot \text{K}^{-1}$  using a van't Hoff analysis. We correct the C-OH bond dissociation energy in acetylacetone, previously determined as 90 kcal·mol<sup>-1</sup> by theory and experiment, to a new value of 121.7 kcal·mol<sup>-1</sup>. Our experiments and electronic structure calculations provide evidence that some of the product channels, including phototautomerization, occur on S<sub>0</sub>, while others likely occur on excited triplet surfaces. Although the large oscillator strength of the  $S_2 \leftarrow S_0$  transition results from the  $(\pi\pi^*)$  excitation of the C=C-C=O backbone, similar to conjugated polyenes, the participation of triplets in the dissociation pathways of acetylacetone appears to have more in common with ketone photochemistry.

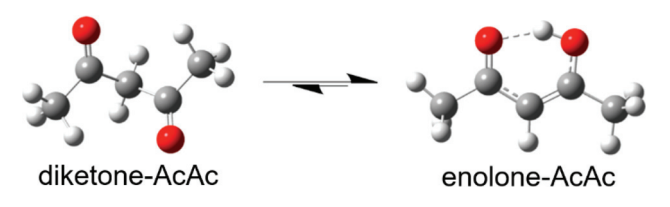
#### 1. INTRODUCTION

The absorption of light by organic molecules and the subsequent energy transformation and release are fundamental process governing life on earth. The photosynthetic fixation of carbon, the chemical basis of vision, <sup>1,2</sup> protection of DNA from ultraviolet damage, and processing of organic aerosols in the Earth's atmosphere<sup>3</sup> all depend on the molecular response to photoexcitation. Photodynamics in these natural systems also enable human efforts in energy harvesting and storage, water splitting, and CO2 reduction. In almost all these systems, the energy deposited in the initially excited electronic state couples to other states of the molecule, causing large-amplitude nuclear and electronic motion, possibly leading to chemical bond breaking. Obtaining a complete view of these phenomena is challenging because a single experiment usually cannot probe all facets of the dynamics. Model systems that display characteristics of broader chemical classes are therefore useful for deep exploration, ideally by multiple experimental and theoretical approaches. Alkenes and carbonyls are among the

most well-studied photochemical systems, and this article investigates a molecule that has elements from both of these classes.

Acetylacetone (2,4-pentanedione, AcAc, see Scheme 1) is a prototypical  $\beta$ -diketone, a class of molecules that have well-

Scheme 1. Diketone and Enolone Tautomers of Acetylacetone



Received: May 15, 2019 Revised: June 3, 2019 Published: June 5, 2019

<sup>&</sup>lt;sup>†</sup>Combustion Research Facility, Sandia National Laboratories, Livermore, California 94551, United States

<sup>\*</sup>Department of Chemistry, University of the Pacific, Stockton, California 95211, United States

<sup>§</sup>Paul Scherrer Institute, CH-5232 Villigen PSI, Switzerland

proven synthetic utility as metal chelating agents<sup>4,5</sup> with potential for low environmental impact<sup>6</sup> and waste degradation. All simple ketones may tautomerize to the enol form, which is usually less stable than the keto form. However, in AcAc and other  $\beta$ -diketones, the diketone form is less stable than the enolone tautomer. <sup>8–10</sup> The dominance of the enolone over diketone was first determined by Meyer<sup>8</sup> in 1912 in liquids and later confirmed in the gas phase by Conant and Thompson<sup>9</sup> in 1932, who measured an enolone:diketone ratio of 92:8 at 295 K. There are two primary reasons for the greater stability of the enolone. First, a strong internal hydrogen bond between the enol hydrogen and the carbonyl oxygen stabilizes the enolone, leading to a structure in which all heavy atoms lie in one plane. Second, conjugation of the C=C and C=O double bonds provides additional stabilization that is not possible in the diketone. Dannenberg and Rios<sup>11</sup> calculated that the H-bond stabilizes the enolone by 12.5 kcal·mol<sup>-1</sup>, which is more than expected for resonance-stabilized H-bonds. They suggested that aromatic character arises from the six  $\pi$ electrons in the six-membered -OCCCOH- ring and provides additional stabilization. Although the enolone tautomer is more stable in the gas phase and in nonpolar solvents, the diketone form becomes favored in polar environments. 10,12

A primary motivation for our interest in acetylacetone is the combination of functional groups present in the enolone tautomer, which has structural elements of carbonyls (the C=O bond), alkenes (C=C bond), conjugated polyenes (O=C-C=C  $\pi$  molecular orbitals), and enols (C=C-OH group). The photochemistry of the first three classes has been extensively studied, and we shall consider how these molecules compare to acetylacetone in the Discussion.

The UV absorption spectrum of acetylacetone was first observed by Grossmann  $^{13}$  in 1924 and extended to the vacuum UV by Nakanishi et al.  $^{12}$  The dominant enolone tautomer has a strong, structureless ( $S_2 \leftarrow S_0$ ) transition of  $(\pi\pi^*)$  character with a peak absorption cross section  $^{14}$  of 4.5  $\times$   $10^{-17}$  cm  $^2$  molecule  $^{-1}$  at 262 nm. From temperature-dependent UV spectra, Nakanishi et al. also identified a weak ( $S_1 \leftarrow S_0$ ) transition with ( $n\pi^*$ ) character at  $\sim$ 294 nm, assigning it to diketone-AcAc. Walzl et al.  $^{15}$  used electron energy loss spectroscopy to study both spin-allowed and spin-forbidden transitions in gas-phase AcAc. They assigned an onset for the ( $S_1 \leftarrow S_0$ ) transition at 324 nm, peaking at 307 nm, and observed a transition to a triplet state with an onset at 394 nm and a maximum at 347 nm.

Several groups studied the UV excitation of enolone-AcAc in rare gas and para- $H_2$  cryogenic matrixes. They observed the photoinduced breaking of the internal H-bond and tautomerization to several higher-energy forms, including the diketone. No other products were observed unless  $O_2$  was doped into the matrix. HOH  $X^2\Pi$  radicals were detected by laser-induced fluorescence after UV irradiation of AcAc in the gas phase. Product-state analysis showed that OH was rotationally and vibrationally cold, but with significant translational energy. All authors interpreted the OH as resulting from absorption of a single UV photon, leading to simple bond fission. The C-OH bond strength was experimentally and theoretically determined to be  $\sim 90 \text{ kcal·mol}^{-1}$ . In addition, propyne (CH<sub>3</sub>CCH) was observed via end product analysis in one study, and signal attributed to CH<sub>3</sub> radicals was detected in another.

The excited-state dynamics of AcAc were directly investigated using a femtosecond UV pump pulse with ultrafast electron diffraction,  $^{25}$  photoelectron spectroscopy,  $^{24,26}$  photoionization mass spectrometry,  $^{24}$  and soft X-ray absorption probing.  $^{27}$  These studies all assumed one-photon excitation of the enolone form to the S $_2$  ( $\pi\pi^*$ ) state, followed by coupling to the lower-lying S $_1$  ( $n\pi^*$ ), T $_2$  ( $n\pi^*$ ), T $_1$  ( $\pi\pi^*$ ), and S $_0$  states. However, they reached conflicting conclusions for the time scale for intersystem crossing (ISC) to triplet states and which dynamical pathways were involved. There have also been theoretical treatments of the dynamics on these coupled electronic states,  $^{24,28}$  including the assertion  $^{24}$  of a roaming pathway.  $^{29}$  A more detailed description of previous studies on the photochemistry and photodynamics of AcAc is presented in the Discussion.

In this paper we excite enolone-AcAc at 266 and 248 nm using nanosecond pulsed lasers and probe the ensuing product formation by three time-resolved methods: (1) multiplexed vacuum ultraviolet (VUV) photoionization mass spectrometry, (2) VUV photoelectron photoion coincidence spectroscopy, and (3) infrared (IR) absorption spectroscopy of OH  $X(^2\Pi)$ . The photochemistry of enolone-AcAc is much more complex than reported earlier. In agreement with previous work, OH is undoubtedly produced following excitation at 266 and 248 nm. However, we provide experimental and theoretical evidence to conclusively demonstrate that OH production is not thermodynamically allowed following one-photon absorption. We show that the  $(S_2 \leftarrow S_0)$  transition is easily saturated, encouraging multiphoton excitation. We measure the enolone: diketone equilibrium constant as a function of temperature and show that photoinduced tautomerization to the diketone is in fact a major process in the gas phase. We quantify numerous additional products and assign them to one-photon or twophoton photochemical channels from enolone-AcAc, on the basis of excitation laser fluence dependence. We derive the channel-specific experimental yields and interpret the results with help from calculated stationary points on the S<sub>0</sub> potential energy surface.

# 2. EXPERIMENTAL AND COMPUTATIONAL METHODS

We studied acetylacetone photochemistry in laser photolysis flow reactors with complementary time-resolved techniques: photoionization mass spectrometry (PIMS), photoelectronphotoion coincidence (PEPICO) spectroscopy, and IR laser absorption. Both PIMS and PEPICO are photoionization methods that enable product assignment using exact mass (e.g.,  $C_3H_6O$ , m/z = 58.042, vs  $C_2H_2O_2$ , m/z = 58.006) and photoionization (PI) or threshold photoelectron (TPE) spectra. We quantified isomer-specific yields (e.g., 1-propen-2-ol, CH<sub>3</sub>C(OH)CH<sub>2</sub> vs acetone, CH<sub>3</sub>COCH<sub>3</sub>) by PIMS, using independently measured absolute PI cross sections from our group and others.<sup>30–35</sup> We further refined our product identification by PEPICO, especially when multiple isomers were present at the same mass. TPE spectra accentuate vibrational progressions that are often obscured in PI spectra; therefore, PEPICO offers better molecular fingerprints than does PIMS. Although product quantification by PEPICO is not possible due to the lack of known absolute cross sections, PEPICO is already a proven tool for identifying elusive intermediates in harsh reaction environments, from flames to pyrolysis and catalysis.<sup>36–44</sup> Lastly, we quantified hydroxyl formation by direct IR laser absorption, which has higher time

Table 1. Summary of Experimental Conditions in the Study of Acetylacetone Photochemistry

	P, Torr	<i>T</i> , K	[AcAc], 10 <sup>12</sup> ·cm <sup>-3</sup>		photolysis fluence, mJ·cm <sup>-2</sup>		::				
	P, Torr	1, K	[AcAc], 10 ·cm	photolysis $\lambda$ , nm	photolysis fluence, mj·cm	probe method	ionization energy, eV				
Tautomeric Equilibrium Measurement											
	10	320-600	12-22			PIMS	8.7-11				
	0.75	300	22			PEPICO	8.6-10.45				
Product Identification											
	10	300	1.8	248	12 and 70	PIMS	8.7-11, 13.58				
				266	30	PIMS					
	0.75	300	22	266	38	PEPICO	8.6-10.45				
	10	295	100	266	30	IR					
Laser Fluence Dependence of Product Yields											
	10	300	7	248	12-108	PIMS	9.5, 10.2, 10.5, 11				
	10	295	100	266	8-72	IR					

resolution than the PIMS and PEPICO instruments and is thus more sensitive to very short-lived OH radicals. Table 1 gives an overview of experimental conditions, with details of our experimental and computational methods presented below.

2.1. Multiplexed Photoionization Mass Spectrometry (PIMS). The photoionization mass spectrometry experiments utilized the multiplexed PIMS apparatus (the low-pressure Sandia Kinetics endstation), <sup>32,45</sup> coupled to the monochromator-equipped T3 terminal of the Chemical Dynamics Beamline 9.0.2 at the Advanced Light Source. Briefly, reactions were initiated at 10 Hz by pulsed photolysis of AcAc in a 62 cm long, 1.05 cm inner diameter (i.d.) flow tube using either the fourth harmonic of an Nd:YAG laser (266 nm, 6 ns pulse width) or the output of a KrF excimer laser (248 nm, 15 ns pulse width, 12-108 mJ·cm<sup>-2</sup> fluence). Acetylacetone (≥99.5% pure) was seeded in excess He by precision mass flow controllers and delivered to the reactor at T = 300-600 Kand P = 10 Torr. The gas mixture was replenished between laser pulses. The gas was continuously sampled through a 650  $\mu$ m diameter orifice in the reactor wall, ionized by tunable narrow-band VUV photons, and analyzed by a 50 kHz pulsed time-of-flight (TOF) mass spectrometer. Time-resolved mass spectra up to  $m/z \sim 160$  were acquired every 20  $\mu$ s for each laser shot over a range of ionization energies E and normalized to the VUV photon flux, measured by a calibrated SXUV-100 photodiode. From the resulting 3-D data set, I(m/z, t, E), energy-resolved time traces and time-resolved PI spectra can be obtained. The overall time resolution, limited mainly by the velocity spread of the sampled neutral species, is ~0.3 ms.

We measured the mass-dependent instrument sensitivity daily with calibrated gas mixtures (0.1% ethene, 0.1% propene, 0.1% 1-butene or 10%  $\rm H_2$ , 1%  $\rm CH_4$ , 0.5% Ar, 0.1% Kr, 0.1% Xe), diluted in excess He. To quantify the reaction products, we compared the observed PI spectra or single-energy ion signals to known absolute PI cross sections, when available. The PI spectra of ion peaks containing signals from multiple isomers were fit to weighted sums of absolute PI spectra of the contributing species. A complete description of the analysis procedure has been published previously.  $^{35,46}$ 

**2.2.** Photoelectron-Photoion Coincidence (PEPICO). Photoelectron-photoion coincidence experiments employed the CRF-PEPICO (Combustion Reactions Followed by Photoelectron Photoion Coincidence) experimental apparatus<sup>47</sup> at the VUV beamline<sup>48</sup> of the Swiss Light Source. Briefly, the setup consists of a side-sampled photolysis reactor, similar to the PIMS instrument. In the present experiments mass flow controllers delivered AcAc (≥99.5% pure) in a large excess of Ar bath gas to the 57.4 cm long, 1.05 cm i.d. halocarbon wax-

coated quartz flow tube at T = 300 K and P = 0.75 Torr. Photolysis radiation from the fourth harmonic of an Nd:YAG pulsed laser (266 nm, 6 ns pulse width, with fluence of 38 mJ· cm<sup>-2</sup> and 20 Hz repetition rate) propagated along the reactor axis. Reaction products were sampled into the PEPICO ionization region through a 400- $\mu$ m pinhole at the halfway point of the flow tube, and the reaction mixture was replenished before the next laser pulse. Focused synchrotron radiation with energy resolution of 3-5 meV, dispersed by a VUV grating, continuously ionized the expanding plume of the sampled neutral gas. A constant, 125 V·cm<sup>-1</sup> electric field was used to extract photoelectrons and photoions in opposite directions from the interaction volume. Cations and electrons were velocity-map imaged (VMI) onto two DLD40 Roentdek position-sensitive delay-line detectors using individually addressable electrode plates that fulfilled both VMI and space-focusing conditions. Plotting the number of recorded coincidences between threshold (near zero kinetic energy) photoelectrons<sup>49</sup> and ions in chosen time-of-flight windows results in mass-selected TPE spectra. The spectra were normalized by the photon flux, measured by a calibrated SXUV-100 photodiode, and corrected for the 67 cm<sup>-1</sup> (ca. 8 meV) red-shift<sup>50</sup> resulting from the continuous extraction field. The overall time resolution of the experiment, limited primarily by the velocity spread of the sampling expansion, is

**2.3.** Transient IR Absorption. OH production from photolysis of acetylacetone was quantified by continuous-wave (CW) direct IR laser absorption in a photolysis flow reactor, coupled to a multipass cell as described previously. 51,52 Briefly, acetylacetone (≥99.5%) vapor was entrained in a flow of He (99.999%) buffer gas in a temperature-stabilized glass bubbler and mixed with additional He by precision mass flow controllers to achieve the desired acetylacetone concentrations. The flow passed through a 1.6-m long, 4 cm i.d. quartz flow cell at T = 295 K and total P = 10 Torr. The AcAc/He gas mixture was excited by the fourth harmonic of an Nd:YAG laser (266 nm, 6 ns pulse width), directed along the central axis of the flow cell. The photolysis fluence was varied from 8 to 72 mJ·cm<sup>-2</sup> for power-dependence measurements, and laser attenuation due to absorption by acetylacetone was measured for each experiment. The reactor was incorporated into a Herriott-type multipass absorption cell with gold end-mirrors, operating in the mid-IR range. CW probe radiation at 2869.7705 nm (1 mW power) from a single-mode distributed feedback laser was used to continuously monitor the P(2.5) f-f rotational transition<sup>53</sup> of the fundamental OH stretch in the electronic ground state of hydroxyl. After mode matching

The Journal of Physical Chemistry A

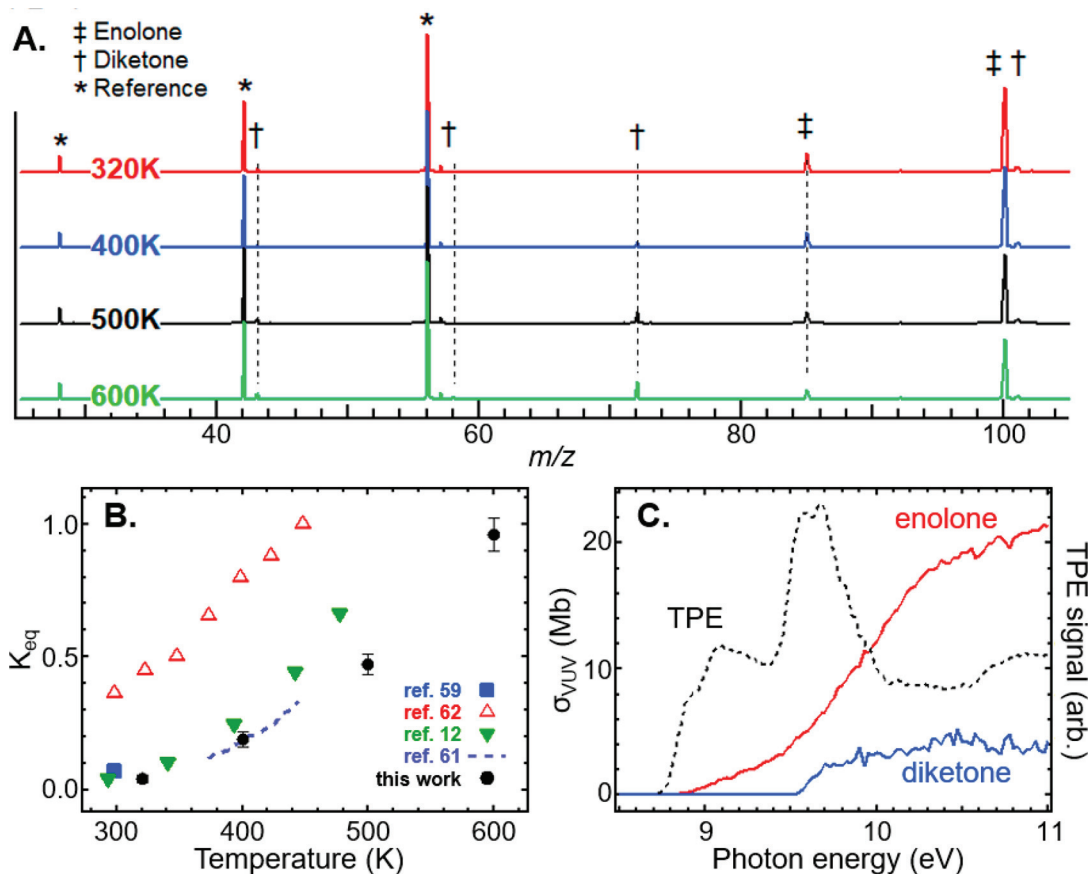


Figure 1. Panel A: photoionization mass spectra of acetylacetone at T=320-600 K, integrated over photon energies 8.7-11 eV. Peaks marked with \* are due to reference compounds (ethene, propene, and 1-butene), † - assigned to diketone-AcAc, ‡ - assigned to enolone-AcAc. Panel B: keto—enol equilibrium constant of AcAc determined in this work, along with literature values from Nakanishi et al., <sup>12</sup> Briegleb and Strohmeyer, <sup>59</sup> Folkendt et al., <sup>61</sup> and Schweig et al. <sup>62</sup> Panel C: absolute PI spectra of diketone- and enolone-AcAc (left axis), along with a relative TPE spectrum of AcAc at 300 K ( $\sim$ 97% enolone, right axis).

lenses, the probe light made a total of 25 passes in the Herriott cell and was detected by a liquid nitrogen-cooled InSb detector. The full OH time trace was recorded for each photolysis laser shot with time resolution  $\leq 1~\mu s$ . Time-resolved OH radical concentration was calculated by Beer's law from the measured attenuation of probe intensity, using line strength and profile parameters in the HITRAN database. <sup>53</sup>

2.4. Computational Methods. The major photodissociation pathways of acetylacetone were also explored by quantum chemical calculations. The energies of end products and stationary points (minima and saddle points) on the ground electronic state of acetylacetone were computed using the Gaussian 09<sup>54</sup> suite of programs. Adiabatic ionization energies (IE<sub>a</sub>) and photoelectron spectra were calculated for product species if experimental reference spectra are unavailable. Ground-state geometries of neutral and ionic species were optimized at the B3LYP/6-311++G(d,p) theory level and the energies were refined using the CBS-QB3 method.<sup>55</sup> Reaction path and approximate saddle point structures were located by constrained optimizations in which either bond lengths or bond angles were scanned, or by using the synchronous transit-guided quasi-Newton (STQN) method. So To verify reaction paths, intrinsic reaction coordinate (IRC) calculations were carried out starting from the located saddle points. Minima in both the forward and reverse directions were reoptimized to confirm the lowest energy structures. Room temperature photoelectron spectra

were calculated using the Franck-Condon approach as implemented in Gaussian 09 or in the program eZspectrum.<sup>57</sup>

#### 3. RESULTS

3.1. Equilibrium Constant for Diketone-Enolone Tautomerization of Acetylacetone. Acetylacetone, like other  $\beta$ -diketones, <sup>58</sup> preferentially adopts either the diketone or the enolone form, depending on its environment. At room temperature in the gas phase 59,60 or in nonpolar solvents 10 AcAc exists primarily as the enolone. Its photodynamics depend on the initial geometry and may involve phototautomerization; hence, we wish to first understand the equilibrium tautomer distribution and to develop tautomerspecific probing techniques. Previous studies from room temperature to 473 K reported a large spread in the equilibrium constant,  $K_{eq}$ , obtained by various experimental methods (see Figure 1B). To address this discrepancy, we investigated the diketone-enolone equilibrium of AcAc at 320-600 K using PIMS. We recorded photoionization spectra of acetylacetone as a function of temperature and determined the absolute PI cross sections of both tautomers. We find that the VUV ionization cross sections of both tautomers are of the same order of magnitude. In contrast, the peak absorption cross-section of diketone-AcAc is ~34 times weaker than that of the enolone in the 170-340 nm range, 12 making precise quantification of the two tautomers by UV spectroscopy challenging.

Due to a high energy barrier,  $^{28}$  AcAc tautomerization is expected to be slow and was shown to require many minutes in solution at temperatures up to 445 K.  $^{61}$  In our setup, dilute room-temperature AcAc vapor flows into a heated reactor with typical residence times less than 1 s, seemingly not enough to reach thermal equilibrium. However, our experiments with varying gas flow velocity revealed that tautomerization was complete for residence times  $\geq$ 100 ms in the flow cell. Because this time scale is too short for pure gas-phase tautomerization, we attribute it to heterogeneous conversion on reactor walls. Although wall-assisted tautomerization clearly accelerates the approach to thermal equilibrium, it does not alter the resulting gas-phase tautomer distribution, enabling reliable quantification of  $K_{\rm eq}$ .

The top panel of Figure 1 shows mass spectra of acetylacetone at 320, 400, 500, and 600 K, integrated over photoionization energies 8.7-11 eV. The mass spectra contain the parent ion peak at m/z = 100 and daughter ions at lighter masses due to dissociative ionization (DI) of AcAc, along with peaks at m/z = 28, 42, and 56 from reference compounds ethene, propene, and 1-butene. These reference species with known PI spectra are added at specific concentrations to the gas flow to enable the quantification of the PI cross-section of both AcAc tautomers.

We find that the parent ion peak in Figure 1 contains enolone and diketone contributions, whereas the daughter ions are due solely to either the enolone (m/z = 85) or the diketone (m/z = 43, 58, 72), on the basis of three observations. First, the shape of the parent ion PI spectrum depends strongly on temperature, clearly indicating a mixture of at least two components, whereas the shapes of the daughter ion spectra do not (see Figure S1). Second, ion TOF spectra from the PEPICO apparatus show a broad shoulder on the right side of the m/z = 85 peak, whereas the m/z = 43, 58, and 72 peaks are narrow and symmetric (Figure S2). This indicates the presence of two neutral AcAc tautomers that fortuitously have very different rates of dissociative ionization, creating these distinct signatures. The broadening of daughter ion peaks in the PEPICO setup is due to the parent ion dissociating on the same microsecond time scale as ion extraction, whereas DI that is much faster than ion extraction results in narrow peak shapes. (Note that the TOF spectra in Figure 1A do not exhibit a peak-shape signature of slow DI at m/z = 85, because unlike PEPICO, the PIMS apparatus uses time-delayed orthogonal ion extraction.) Lastly, the m/z = 85 intensity decreases with increasing T, whereas that of m/z = 43, 58, and 72 daughter ions increases with increasing T because of the shift in  $K_{eq}$  away from enolone-AcAc in favor of the higherenergy diketone tautomer.

To determine  $K_{\rm eq}$ , we used the T-dependent ion signals from m/z=72 and 85 peaks as proxies for the diketone and enolone populations, respectively. The PI spectra of these peaks show essentially no thermal broadening (Figure S1), suggesting that partial PI cross sections into these fragment ions do not depend on T. Defining  $K_{\rm eq}=[{\rm diketone}]/[{\rm enolone}]$ , the molar fractions of diketone and enolone are

$$\frac{[\text{diketone}]}{[\text{diketone}] + [\text{enolone}]} = \frac{K_{\text{eq}}}{1 + K_{\text{eq}}} \tag{1a}$$

$$\frac{\text{[enolone]}}{\text{[diketone]} + \text{[enolone]}} = \frac{1}{1 + K_{\text{eq}}}$$
(1b)

Because PIMS signals at m/z = 72 ( $S_{72}$ ) and 85 ( $S_{85}$ ) are proportional to the concentrations of diketone and enolone, respectively, the ratio of molar fractions of a given tautomer at temperatures  $T_1$  and  $T_2$  is

$$\frac{S_{72}^{(T_1)}}{S_{72}^{(T_2)}} = \frac{[\text{diketone}](T_1)}{[\text{diketone}](T_2)} = \frac{K_{\text{eq}}^{(T_1)}}{K_{\text{eq}}^{(T_2)}} \cdot \frac{1 + K_{\text{eq}}^{(T_2)}}{1 + K_{\text{eq}}^{(T_1)}}$$
(2a)

$$\frac{S_{85}^{(T_1)}}{S_{85}^{(T_2)}} = \frac{[\text{enolone}](T_1)}{[\text{enolone}](T_2)} = \frac{1 + K_{\text{eq}}^{(T_2)}}{1 + K_{\text{eq}}^{(T_1)}}$$
(2b)

The mass spectra at four different temperatures in Figure 1A yield 12 possible T-dependent ratios: 6 for the diketone (eq 2a) and 6 for the enolone (eq 2b). Together this results in an overdetermined system of 12 equations with 4 unknowns (the values of  $K_{\rm eq}$  at the four temperatures), which was solved by least-squares minimization. The fitted values  $K_{\rm eq} = 0.042 \pm 0.012$ ,  $0.19 \pm 0.03$ ,  $0.47 \pm 0.04$ , and  $0.96 \pm 0.06$  at T = 320, 400, 500, and 600 K, respectively, are plotted in Figure 1B along with earlier literature results. Our results enable a van't Hoff analysis to determine the enthalpy and entropy change of tautomerization and to extrapolate  $K_{\rm eq}$  to 300 K. The details of this analysis are presented in section 4.3, resulting in  $K_{\rm eq}(300 \, {\rm K}) = 0.03 \pm 0.003$ ; i.e., the equilibrium molar fraction of diketone-AcAc at 300 K is  $(2.9 \pm 0.3)\%$ 

Our measurement of  $K_{\rm eq}$  also allows us to decompose the PI spectrum of acetylacetone at m/z=100 into its individual tautomeric contributions. The PI signal  $S_i(E)$  due to species i is

$$S_i(E) = A \cdot [i] \cdot \sigma_i(E) \tag{3}$$

where A is an instrumental factor that is constant for a given m/z ratio, [i] is the concentration of neutral species i in the reactor, and  $\sigma_i(E)$  is the PI cross section at photon energy E. The total signal at m/z=100,  $S_{100}(E,T)$ , has contributions from both neutral tautomers and varies with temperature because the concentrations of the two tautomers vary with temperature. We define an effective absolute PI cross section  $\sigma_{100}^{\rm eff}(E,T)$  that is a concentration-weighted sum of the cross sections of both tautomers.

$$\sigma_{100}^{\text{eff}}(E,T) \equiv \frac{[\text{enolone}](T) \cdot \sigma_{100}^{\text{en}}(E) + [\text{diketone}](T) \cdot \sigma_{100}^{\text{di}}(E)}{[\text{enolone}](T) + [\text{diketone}](T)}$$
(4)

where  $\sigma^{\rm en}_{100}(E)$  and  $\sigma^{\rm di}_{100}(E)$  are the temperature-independent cross sections of each tautomer that we seek to extract. We measure  $\sigma^{\rm eff}_{100}$  by comparing the PI spectrum of AcAc with that of propene, a reference species with known concentration and cross-section. With  $\sigma^{\rm eff}_{100}(E,T)$  and  $K_{\rm eq}(T)$  in hand, we substitute eqs 1a and 1b into eq 4 to yield

$$\sigma_{100}^{\text{eff}}(E,T) = \frac{1}{1 + K_{\text{eq}}(T)} |\sigma_{100}^{\text{en}}(E)| + \frac{K_{\text{eq}}(T)}{1 + K_{\text{eq}}(T)} |\sigma_{100}^{\text{di}}(E)|$$
(5)

From eq 5 we have four functions of E (one for each temperature) that are solved simultaneously by least-squares minimization to yield the two T-independent functions  $\sigma_{100}^{\rm en}(E)$  and  $\sigma_{100}^{\rm di}(E)$ . The absolute value operator enforces the physically meaningful nonzero value of the cross sections. Without it, the result is very similar, except that  $\sigma_{100}^{\rm di}(E)$  acquires small negative values at some points below its ionization onset due to the noise in the experimental data.

The resulting absolute PI cross sections of diketone- and enolone-AcAc are tabulated in Table ST1 and shown in Figure 1C. The CBS-QB3 calculated IE, of the enolone is 8.88 eV, which matches well the observed onset at ~8.9 eV. In contrast, the calculated diketone IE, is 9.13 eV, whereas the observed onset is at ~9.5 eV. Calculations of the diketone-AcAc neutral and cation potential energy surfaces (PES) revealed a large geometry change in the relative orientation of the two C=O groups upon ionization to the global cation minimum. The calculations also indicate the presence of a local energy minimum on the cation PES, which lies 0.4 eV above the global minimum and is close to the relaxed neutral diketone geometry (see Figure S8). Qualitatively, this suggests that the onset region of the diketone PI spectrum should be dominated by transitions to the higher-energy cation conformer, resulting in a relatively sharp ionization onset ~0.4 eV above the IE<sub>3</sub>, in excellent agreement with the extracted diketone spectrum in Figure 1C. The difference in the PI onsets means that the parent ion signal of AcAc below 9.5 eV arises only from the enolone. The T-dependence of the intensity of this low-energy portion of the spectrum matches that of the m/z = 85 daughter ion, confirming that this daughter ion is due solely to the enolone.

**3.2. Photoproduct Identification.** We studied the photochemistry of acetylacetone by complementary timeresolved PIMS, PEPICO, and IR absorption methods, as shown in Table 1. The main PIMS experiments aimed at product discovery were performed with  $[AcAc] = 1.8 \times 10^{12}$ cm<sup>-3</sup> in a He bath at 10 Torr and 300 K, using 266 nm excitation with a fluence of 30 mJ·cm<sup>-2</sup> and 248 nm excitation (12 and 70 mJ·cm<sup>-2</sup>). Supporting PIMS studies at 500–600 K or in the presence of  $O_2$  (2.8 ×  $10^{16}$  cm<sup>-3</sup>) aided in product assignment. Products were identified by their PI spectra in the 8.7-11 eV range or by single-energy ionization at 13.58 eV and confirmed by TPE spectra over 8.6-10.45 eV. The excitation fluence dependence of products was also quantified by PIMS at 248 nm in the range 12-108 mJ·cm<sup>-2</sup>, as described in section 3.3. Lastly, hydroxyl radicals were quantified by IR absorption at 10 Torr and 300 K after 266 nm excitation with fluences of 8-72 mJ·cm<sup>-2</sup> per pulse.

Figure 2 shows typical OH time profiles, expressed as absolute OH concentrations (left axis) or as percentage of the initial AcAc concentration (right axis). All OH signals have

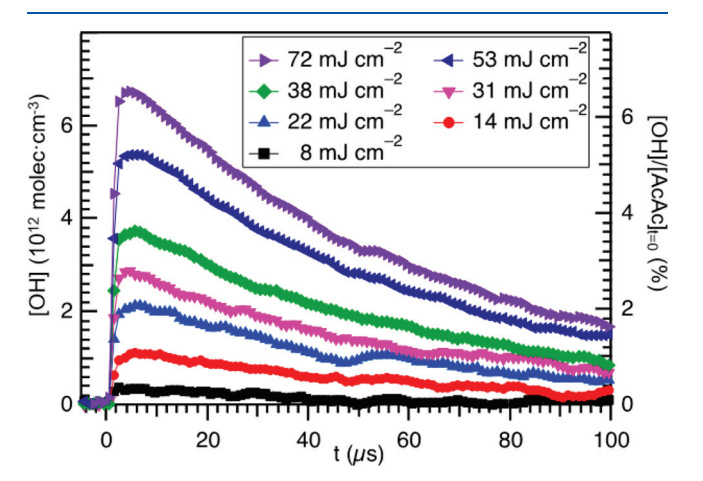


Figure 2. IR absorption measurements of OH radicals, produced by 266 nm photolysis of AcAc  $(1 \times 10^{14} \text{ molecules cm}^{-3})$  in a He bath at 295 K and 10 Torr, using photolysis fluences of 8–72 mJ·cm<sup>-2</sup>.

instrument-limited rises, followed by decays with time scale of tens of microseconds due to wall losses and to the reaction with AcAc. The photolytic OH yield was determined at each laser fluence by extrapolating the time profiles back to t=0.

Figure 3 shows representative transient mass spectra, acquired by PIMS at 300 K and 10 Torr, using 248 nm photolysis with fluence of 70 mJ·cm<sup>-2</sup>. The main spectrum in panel A was integrated over kinetic time t = 0-40 ms and photoionization energies E = 8.7-11 eV. Inset B is a portion of the mass spectrum integrated over t = 0-10 ms and E = 8.7-11 eV; inset C shows another portion of the mass spectrum, acquired with E = 13.58 eV. The prephotolysis signals in all mass spectra were subtracted, revealing numerous laserinduced ion peaks. The negative transients at m/z = 85 and 100 indicate the removal of enolone-AcAc, whereas the positive peaks indicate the formation of products. Mass spectra, obtained by PEPICO, were consistent with PIMS (see Figure S3). In all, we detected 14 time-resolved ion peaks (m/z = 15, 16, 18, 29, 39, 40, 42, 43, 58, 72, 82, 84, 85, and100) that we assigned to 15 unique products of AcAc photochemistry through spectroscopic measurements and quantum chemical calculations of possible photochemical pathways. These products are summarized in Table 2, and details of the analysis are given below and in the Supporting Information.

The m/z=85 ion peak is due only to the DI of enolone-AcAc. The m/z=100 peak is also dominated by the signal from the enolone at 300 K because (1) it is present in 97.1% molar fraction, (2) it has a larger PI cross-section than the diketone, and (3) the photoinduced yield of diketone is smaller than unity, as seen in Table 2. As a result, the transient signals at m/z=85 and 100 are essentially all due to the depletion of enolone-AcAc. They have instrument-limited depletion times and no additional signal decays, as shown in Figure S6, consistent with no reactivity after the prompt depletion. The initial AcAc concentrations in the reactor are known, so the fractional depletion of these peaks quantifies the concentration of enolone removed by laser excitation at each experimental condition.

Figure 4A plots the time trace of the m/z=72 peak after 248 nm excitation at a fluence of 70 mJ·cm<sup>-2</sup>, showing prephotolysis signal and additional laser-induced signal after t=0. As discussed in section 3.1, prior to photolysis the m/z=72 ions arise solely from diketone-AcAc, which at 300 K is present at 2.9% molar fraction: [diketone] =  $5.2 \times 10^{10}$  molecules·cm<sup>-3</sup>. Figure 4B shows that the PI spectra of this peak, integrated over t=-10 to -1 ms and t=1-10 ms (scaled by 0.33), are identical. This shows that although in principle the laser-induced signal at m/z=72 could be due to many compounds with the formula  $C_4H_8O$ , here it comes only from the DI of additional diketone, produced from enolone by the 248 nm laser pulse. The ratio of post- vs pre-excitation signals directly quantifies the diketone concentration produced in each experiment.

The transient peaks at m/z = 16 (CH<sub>4</sub>) and 18 (H<sub>2</sub>O) were assigned to methane and water and quantified via their absolute cross sections <sup>63,64</sup> by single ionization energy measurements at E = 13.58 eV. No other isomers with these formulas exist, and DI of larger species into CH<sub>4</sub><sup>+</sup> and H<sub>2</sub>O<sup>+</sup> fragments can be ruled out due to the high ionization energies of these small molecules: 12.61 and 12.62 eV, respectively. <sup>65</sup> Six more peaks were assigned by comparing their PI and TPE spectra with known reference standards and quantified via

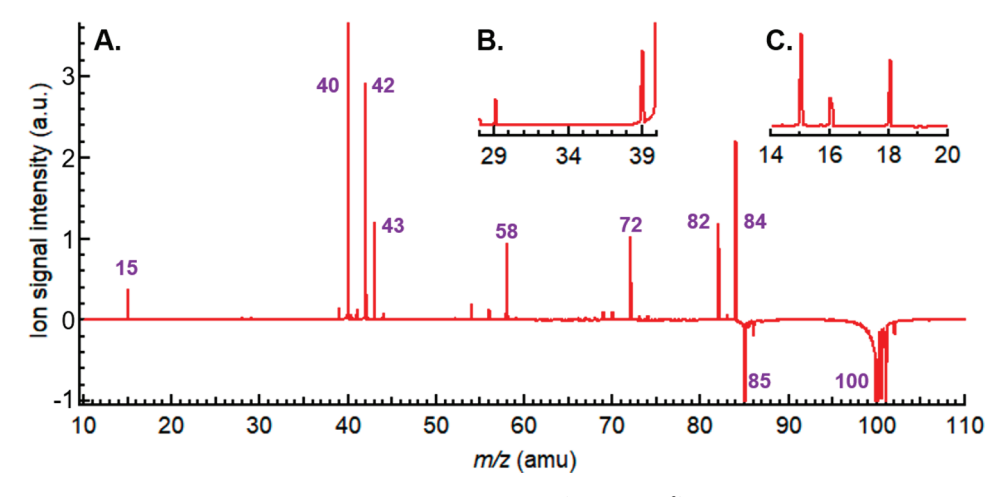


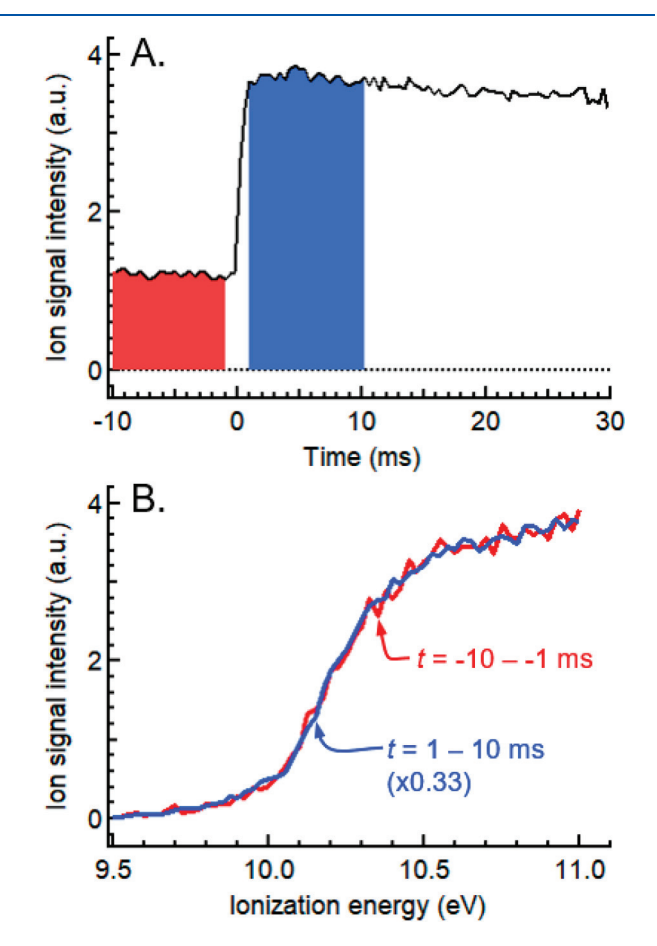
Figure 3. Transient mass spectra, acquired by PIMS after 248 nm photolysis ( $70 \text{ mJ} \cdot \text{cm}^{-2}$ ) of AcAc in He bath gas at 300 K and 10 Torr. The prephotolysis ion signals were subtracted, so that photoproducts appear as positive peaks and the depletion of enolone-AcAc appears as negative peaks at m/z = 100 and 85. Panel A: full mass spectrum, integrated over t = 0-40 ms and ionization energies E = 8.7-11 eV. Inset B: a portion of the same mass spectrum, 28–40 amu, integrated over t = 0-10 ms. Inset C: a portion of the mass spectrum, 14–20 amu, acquired with E = 13.58 eV and integrated over t = 10-40 ms.

Table 2. Acetylacetone Photoproducts at 300 K and 10 Torr  $([AcAc]_{t=0} = 1.8 \times 10^{12} \text{ cm}^{-3})^a$ 

			product		
m/z	sum formula	assignment	one- photon	two- photon	product channel
15.023	$CH_3$	methyl	$0^{+0.7}_{-0}$	$27 \pm 4$	
16.031	$CH_4$	methane			II
	OH	hydroxyl	$0^{+2}_{-0}$	$21 \pm 4$	
18.011	$H_2O$	water			III
29.039	$C_2H_5$	DI of acetonyl			VI
39.023	$C_3H_3$	propargyl	$0^{+0.3}_{-0}$	$3.4 \pm 2$	
40.031	$C_3H_4$	allene	$0^{+0.1}_{-0}$	$1_{-1}^{+2}$	
		propyne	$0^{+0.4}_{-0}$	$25 \pm 3$	
42.011	$C_2H_2O$	ketene	$2^{+4}_{-2}$	$16 \pm 6$	IV/V
43.018	$C_2H_3O$	DI of diketone			Ι
		acetyl	$5 \pm 4$	$0^{+5}_{-0}$	VI
58.042	$C_3H_6O$	DI of diketone			I
		1-propen-2- ol	$3.7 \pm 1.6$	$1_{-1}^{+2}$	IV
		acetone	$3 \pm 1.4$	$0.8^{+2}_{-0.8}$	V
72.058	$C_4H_8O$	DI of diketone	$29 \pm 4$	$0^{+2}_{-0}$	I
82.042	$C_5H_6O$	acetyl allene	$25 \pm 4$	$0^{+2}_{-0}$	III
84.021	$C_4H_4O_2$	acetyl ketene	12 ± 4	$0^{+4}_{-0}$	II
85.029	$C_4H_5O_2$	DI of enolone			
100.052	$C_5H_8O_2$	diketone			I
		enolone			

"OH was detected by IR absorption, methane and water by PIMS, and all other products by PIMS and PEPICO. Product yields in the limit of pure one- or two-photon excitation ( $\Phi_i^{(1)}$  and  $\Phi_i^{(2)}$ ) were derived from the fluence-dependent signals at 266 nm (OH) and at 248 nm (all other species), as described in section 3.3. Photochemical product channels I–VI are assigned only for one-photon products, as described in section 4.4.

absolute PI cross sections: m/z = 15, methyl;<sup>32</sup> 39, propargyl;<sup>32</sup> 40, a mixture of allene<sup>30</sup> and propyne;<sup>33</sup> 42,



**Figure 4.** Panel A: kinetic time profile of the m/z=72 ion peak acquired by PIMS after 248 nm excitation of AcAc at 10 Torr and 300 K, using ionization energies 8.7-11 eV. The shaded areas indicate the pre- and postexcitation time windows: red, t=-10 to -1 ms, and blue, t=1 to 10 ms. Panel B: PI spectra of the m/z=72 peak. The pre-excitation PI spectrum (red) is due to the DI of diketone-AcAc, which is present at 2.9% molar fraction. The postexcitation PI spectrum (blue) is scaled by 0.33.

ketene;<sup>30</sup> 43, acetyl; and 58, a mixture of 1-propen-2-ol and acetone.<sup>35</sup> The absolute PI cross sections of acetyl and 1-

The Journal of Physical Chemistry A

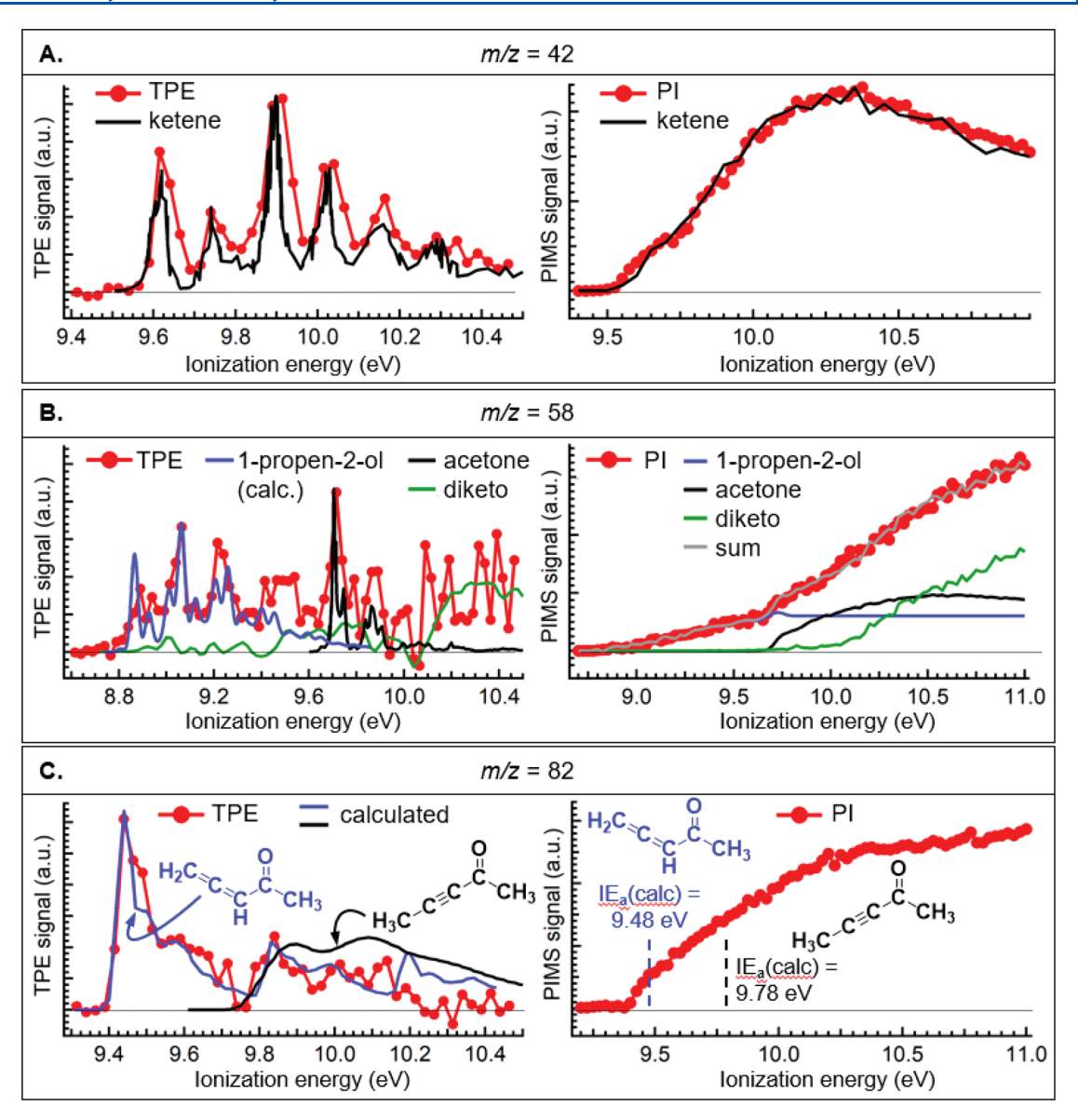


Figure 5. Representative examples of the assignment of AcAc photoproducts (red), observed by PEPICO and PIMS. Panel A: measured transient TPE and PI spectra of m/z = 42 ions; literature TPE<sup>37</sup> and PI<sup>30</sup> spectra of ketene, CH<sub>2</sub>CO. Panel B: transient TPE and PI spectra at m/z = 58; reference TPE spectra of acetone, CH<sub>3</sub>COCH<sub>3</sub>,<sup>66</sup> and diketone daughter ions (this work); calculated TPE spectrum of 1-propen-2-ol, CH<sub>3</sub>C(OH)CH<sub>2</sub> (this work); reference PI spectra of 1-propen-2-ol (this work), acetone,<sup>35</sup> and diketone DI (this work). Panel C: measured transient TPE and PI spectra at m/z = 82; calculated TPE spectra of CH<sub>3</sub>C(O)CHCCH<sub>2</sub> (blue) and CH<sub>3</sub>C(O)CCCH<sub>3</sub> (black). The calculated spectra were shifted by +13 meV.

propen-2-ol were measured by our group recently and are summarized in the Supporting Information. The signals from closed-shell stable products at m/z = 16, 18, 40, 42, and 58 had instrument-limited risetimes to constant plateaus; they were quantified using their average signal at t = 30-40 ms. The signals at m/z = 15, 39, and 43 appeared rapidly and decayed by t = 40 ms, as expected for radicals; they were quantified by extrapolating their signal to t = 0. Examples of our analysis are given in Figure 5; the remaining product assignments and typical time traces are shown in Figures S4–S6.

Figure 5A shows the transient PI and TPE spectra of the m/z = 42.011 (C<sub>2</sub>H<sub>2</sub>O) peak, which has three possible isomers: ketene, ethynol, or oxirene. The literature TPE<sup>66</sup> and PI<sup>30</sup> spectra of ketene match the measured spectra well, indicating that it is the only product at this mass. Figure 5B gives a more complex example of the m/z = 58.042 (C<sub>3</sub>H<sub>6</sub>O) peak with 9

possible isomers: acetone, propanal, oxetane, methyloxirane, cyclopropanol, 1-propen-1-ol, 1-propen-2-ol, 2-propen-1-ol, and methyl vinyl ether. The measured TPE and PI spectra in Figure 5B are reproduced well up to 10 eV by the reference spectra of 1-propen-2-ol and acetone,  $^{35,66}$  whereas nearly all other possible  $\rm C_3H_6O$  species can be ruled out on the basis of their PI<sup>31,35</sup> or TPE<sup>67,68</sup> spectra. The absolute PI spectrum of 1-propen-2-ol was measured in this work (see Table S2), and the TPE spectrum was calculated. The signals above 10 eV are fully fitted by the reference spectra of diketone daughter ions at m/z=58, which bolsters our earlier conclusion that diketone-AcAc is formed by the UV excitation of the enolone.

Figure 5C shows an example of the most challenging case of product identification, for which no literature spectra exist. The  $m/z = 82.042 \, (C_5 H_6 O)$  peak corresponds to a loss of  $H_2 O$  from AcAc, constraining its likely source to plausible

acetyl

m/z = 58

m/z=82

m/z = 84

80

60

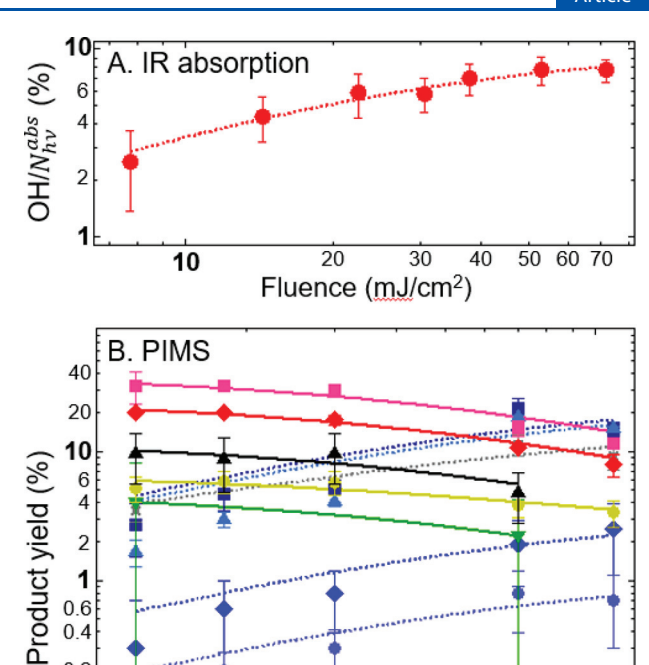
diketo

coproducts of water elimination. Our calculations found transition states for two direct water loss pathways from the enolone, leading to acetyl propyne, CH<sub>3</sub>C(O)CCCH<sub>3</sub>, or acetyl allene, CH<sub>3</sub>C(O)CHCCH<sub>2</sub>. Since no reference spectra for these compounds are available, we compared our experimental results to calculated TPE spectra, using the geometries and vibrational frequencies at the B3LYP level. The onsets of both calculated spectra are in close agreement with the CBS-QB3 calculated IE<sub>a</sub> of 9.48 and 9.78 eV for acetyl allene and acetyl propyne, respectively. The simulated Franck-Condon progressions were shifted in energy by +13 meV to align the onset of the acetyl allene spectrum with the first photoelectron peak at 9.45 eV. After this shift, the simulated acetyl allene spectrum matches the experimental signal nearly perfectly, suggesting that the acetyl propyne contribution is minor, at most.

The peak at m/z = 84.021 (C<sub>4</sub>H<sub>4</sub>O<sub>2</sub>) is likely due to direct elimination of methane from enolone-AcAc. Our quantum chemical calculations identified two low-lying transition states for CH<sub>4</sub> loss, leading to acetyl ketene, CH<sub>3</sub>C(O)CHCO, or hydroxyvinyl ketene, CH<sub>2</sub>C(OH)CHCO. The calculated IE<sub>a</sub> of hydroxyvinyl ketene is 8.24 eV, far below the observed onset of ion signals (9.6 eV), allowing us to rule it out as a coproduct of CH<sub>4</sub>. The calculated IE<sub>a</sub> of acetyl ketene is 9.59 eV, which matches the observed onset; a comparison of the measured and calculated TPE spectra (Figure S4) shows fair agreement.

Lastly, the m/z = 29.039 (C<sub>2</sub>H<sub>5</sub>) PI spectrum does not match the reference spectrum of ethyl,<sup>69</sup> which is the only isomer with this formula. Instead, we assign it to dissociative ionization of the acetonyl radical (CH<sub>3</sub>COCH<sub>2</sub><sup>+</sup> → CH<sub>3</sub>CH<sub>2</sub><sup>+</sup> + CO), on the basis of three observations. First, our CBS-QB3 calculations indicate that vertical ionization from the equilibrium acetonyl geometry accesses a saddle point region on the C<sub>3</sub>H<sub>5</sub>O<sup>+</sup> potential energy surface, from which neutral CO elimination is barrierless and exothermic by about 22 kcalmol<sup>-1</sup> (see Figure S7). Second, earlier studies found that ionization of the related vinoxy radical does not produce a parent cation and instead undergoes CO elimination: HCOCH<sub>2</sub><sup>+</sup> → CH<sub>3</sub><sup>+</sup> + CO.<sup>70</sup> This result agrees with our calculations of the C2H3O+ PES, which found analogous barrierless CO elimination from the vinoxy cation, thus supporting our conclusions for acetonyl. Finally, additional PIMS experiments with 2.8  $\times$  10<sup>16</sup> cm<sup>-3</sup> O<sub>2</sub> added to the sample showed that the m/z = 29 peak disappeared and a peak at m/z = 57 appeared. At these conditions we expect acetonyl to react with O2 to form a stabilized peroxy radical. Most organic peroxy radicals (ROO) undergo dissociative ionization to  $R^+ + O_2^{-71}$  and it is likely that ionization of acetonyl peroxy produces a stable  $C_2H_5O^+$  daughter ion at m/z = 57(presumably with a different structure than the unstable acetonyl cation).

3.3. Laser Excitation Fluence Dependence. As a first step toward understanding AcAc photochemistry, we wish to separate the products of one-photon excitation (mainly to  $S_2$ ), from those of multiphoton excitation to higher-lying electronic states. To address this question, we performed excitation fluence dependence studies using both IR absorption and PIMS detection, as described in Table 1, and the results of these studies are presented in Figure 6. For concurrent oneand two-photon excitation with absorption cross sections  $\sigma_1$ and  $\sigma_2$ , the number densities of depleted AcAc  $(N_D)$  and of absorbed photons  $(N_{h\nu}^{abs})$  can be expressed in terms of laser fluence *F*:



0.6

0.2

0.1

10

Figure 6. Excitation fluence dependence of acetylacetone photoproducts. Panel A: IR absorption probing of OH, following 266 nm excitation in the 8-72 mJ·cm<sup>-2</sup> range. OH yield is calculated relative to the measured density of absorbed photons. Dotted line: leastsquares fit to eq 9. Panel B: PIMS probing of photoproducts after 248 nm excitation in the 12-108 mJ/cm<sup>2</sup> range. Product yields are computed relative to the depleted acetylacetone number density. Solid and dotted lines are fits to eq 10.

20

propargy

allene

propyne

ketene

Fluence (mJ/cm<sup>2</sup>)

40

$$N_{\rm D} = N_0 [1 - \exp(-\sigma_1 F - \sigma_2 F^2)]$$
 (6)

$$N_{h\nu}^{\text{abs}} = N_{\text{D}} \cdot \left( \frac{\sigma_1}{\sigma_1 + \sigma_2 F} + 2 \frac{\sigma_2 F}{\sigma_1 + \sigma_2 F} \right) \tag{7}$$

where  $N_0$  is the number density of AcAc molecules prior to photolysis. The number density of products of species  $i(N_i)$  is the sum of those formed by the one-photon and two-photon

$$N_{i} = N_{i}^{(1)} + N_{i}^{(2)} = N_{D} \cdot \left( \Phi_{i}^{(1)} \frac{\sigma_{1}}{\sigma_{1} + \sigma_{2}F} + \Phi_{i}^{(2)} \frac{\sigma_{2}F}{\sigma_{1} + \sigma_{2}F} \right)$$
(8)

 $\Phi_i^{(1)}$  and  $\Phi_i^{(2)}$  are the fractional yields of product i per AcAc molecule, excited via the one-photon and the two-photon transition, respectively. Note that although  $\Phi_i^{(1)}$  and  $\bar{\Phi}_i^{(2)}$  are physically meaningful product branching fractions following a one- or two-photon transition, they are not equivalent to the experimentally observed yields, except in special cases. The one-photon yield  $\Phi_i^{(1)}$  would be equal to the observed yields of i only in the limit of extremely low fluence (i.e., practically no two-photon excitation), while  $\Phi_i^{(2)}$  would be equal to the observed yields in the limit of very high fluence (i.e., essentially all two-photon excitation).

The Journal of Physical Chemistry A

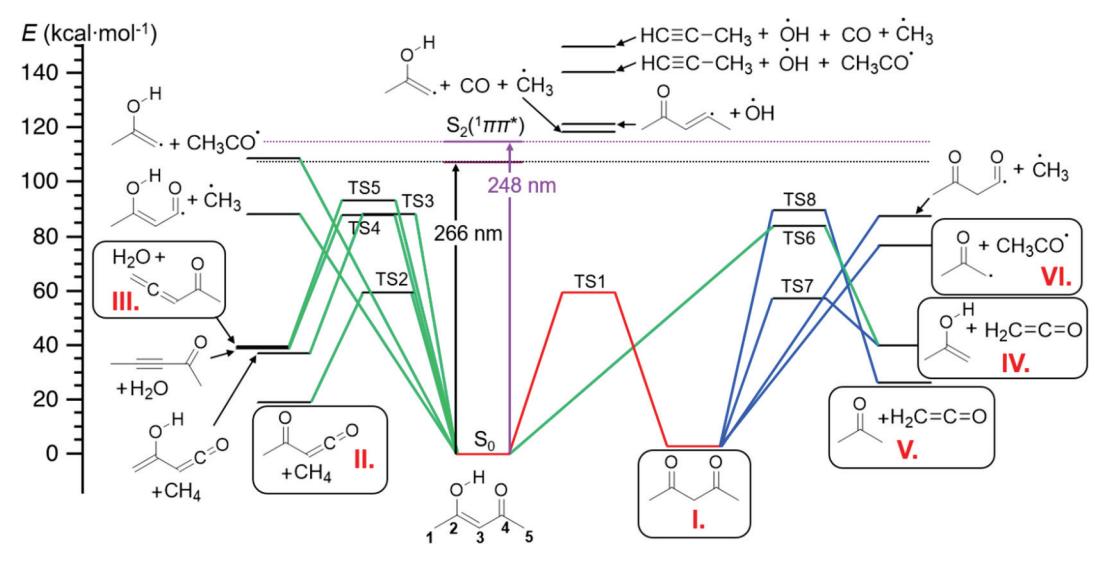


**Figure 7.** Relevant stationary points on the S<sub>0</sub> electronic state of AcAc and key products, calculated at the CBS-QB3 level. Molecular geometries are shown schematically, and the C atom numbering convention is shown for enolone-AcAc. Reaction pathways via transition states TS1–TS8 are marked by solid lines: red (tautomerization), blue (diketone decomposition), green (enolone decomposition). The one-photon 248 and 266 nm excitation energies are shown as dotted lines. Roman numerals I–VI indicate our assignment of observed one-photon pathways.

Figure 6A shows the power dependence of the observed OH signals. IR probing does not measure the depletion of acetylacetone directly. Therefore, we expressed the observed yield  $Y_{\rm OH}$  by dividing the measured OH concentration (extrapolated to t=0) by the measured number density of absorbed 266 nm photons (photons·cm<sup>-3</sup>). Dividing eq 8 by eq 7 and introducing r, the ratio of the two-photon and one-photon absorption cross sections, leads to the expression for  $Y_{\rm OH}$ :

$$Y_{\text{OH}} = \frac{N_{\text{OH}}}{N_{h\nu}^{\text{abs}}} = \frac{\Phi_{\text{OH}}^{(1)} + \Phi_{\text{OH}}^{(2)} \cdot r \cdot F}{1 + 2r \cdot F}; \qquad r = \frac{\sigma_2}{\sigma_1}$$
 (9)

Figure 6A shows a least-squares fit of the OH yields to eq 9, giving  $\Phi_{\rm OH}^{(1)} = 0^{+2}_{-0}\%$ ,  $\Phi_{\rm OH}^{(2)} = 21 \pm 4\%$ , and  $r = (1.8 \pm 1) \times 10^{-17}$  cm<sup>2</sup>·molecule<sup>-1</sup>. In principle, r should allow us to derive the two-photon absorption cross-section of AcAc at 266 nm, on the basis of the reported one-photon cross-section. However, we did not attempt such a derivation because of the inherent assumption in our analysis of no three-photon (or higherorder) excitations. Likewise, the fitted value of 21% OH yield per two-photon excitation of AcAc relies on the same assumption. A detailed study of multiphoton photochemistry of AcAc is outside our present scope, and the main finding from Figure 6A is that the one-photon OH yield is negligible.

Figure 6B shows the fluence dependence of 11 products, detected by PIMS. We quantified methyl, propargyl, allene, propyne, ketene, acetyl, acetone, 1-propen-2-ol, and diketone-AcAc production as described in section 3.2. Acetone and 1-propen-2-ol show the same power dependence; therefore, we sum their yields and display them as m/z = 58 for clarity. Unfortunately, we cannot measure the fluence dependence of acetonyl due to low signals. The absolute PI cross sections of acetyl allene and acetyl ketene at m/z = 82 and 84 are not available; therefore, we obtained their relative signals as a function of laser fluence and translated them into absolute concentrations by scaling them to match the measured number densities of their coproducts,  $H_2O$  and  $CH_4$ , at a fluence of 70 mJ·cm<sup>-2</sup>. The water and methane yields were not measured at

other fluences because their detection is challenging, since it requires high ionization energies.

Our PIMS apparatus cannot measure the photolysis laser absorption, but it does directly measure AcAc depletion. We report the observed product yields  $Y_i$  relative to the depleted enolone concentration in Figure 6B and obtain an expression for their fluence dependence by dividing eq 8 by eq 6:

$$Y_{i} = \frac{N_{i}}{N_{D}} = \frac{\Phi_{i}^{(1)} + \Phi_{i}^{(2)} \cdot r \cdot F}{1 + r \cdot F}$$
(10)

All data in Figure 6B were simultaneously fit to eq 10, using a global cross-section ratio r and individually varied  $\Phi_i^{(1)}$  and  $\Phi_i^{(2)}$ . The optimized  $r = (1.3 \pm 0.1) \times 10^{-17} \text{ cm}^2 \text{ molecule}^{-1}$  at 248 nm, but we again refrain from drawing conclusions about the two-photon absorption cross-section. The fitted one- and two-photon limit yields for all products in Figure 6 are included in Table 2. The key finding is that like OH, the production of methyl, propargyl, allene, and propyne is solely multiphoton. The concentrations of these products relative to the depleted AcAc concentration grow dramatically with increasing excitation fluence. The formation of diketone, acetyl, acetyl allene, and acetyl ketene is purely one-photon. Their signals relative to depleted AcAc decrease at high fluence because the fraction of two-photon excited enolone increases. Acetone and 1-propen-2-of had mixed fluence dependence, with  $\Phi_i^{(1)} = 3\%$  and 3.7% and  $\Phi_i^{(2)} = 0.8\%$  and 1%, respectively. Ketene also showed mixed behavior, more heavily weighted toward multiphoton excitation, with  $\Phi_i^{(1)} = 2\%$  and  $\Phi_i^{(2)} =$ 

**3.4. Quantum Chemical Calculations of Acetylacetone Photochemical Pathways.** To help interpret the complex photoproducts of acetylacetone, we calculated the energies of relevant dissociation products and stationary points on the ground  $(S_0)$  electronic state. Figure 7 and Table S2 show our computed energy barrier for enolone—diketone tautomerization (TS1) and stationary points for 10 decomposition reactions. Six of these reactions are concerted isomerization—dissociation processes that have energy barriers, associated with transition states TS2—TS10. (Two of the

calculated barriers, TS9 and TS10, are omitted from Figure 7 for clarity.) We carried out IRC scans starting at each saddle point to elucidate the reaction end products. We also characterized four Norrish type I reactions, corresponding to the breaking of the  $C_3-C_4$  or  $C_4-C_5$  bond in the diketone and enolone. Relaxed optimization scans along the minimum energy path of these reactions confirmed that they have no barriers on S<sub>0</sub>, as is expected for simple bond cleavage to form two radical products. The energies of one-photon 248 and 266 nm excitation (107.5 and 115.3 kcal·mol<sup>-1</sup>, respectively) are shown in Figure 7, and optimized TS geometries are available in the Suporting Information.

#### 4. DISCUSSION

Our experiments reveal much richer gas-phase photochemistry of AcAc than did previous reports. To place our results in context, we first review this literature. Next, we consider how our findings compare to what is known about molecules with structural motifs found in AcAc: carbonyls, alkenes, conjugated polyenes, and enols. Given this background, we then discuss the implications of our results on the keto-enol equilibrium and thermodynamics, and on the pathways of one- and twophoton photochemistry. Last, we suggest experimental and theoretical studies to address outstanding questions.

4.1. Previous Literature Studies of Enolone-AcAc Photochemistry and Dynamics. The first photochemistry study by Roubin et al. 18 photolyzed acetylacetone in a cryogenic Xe matrix at 230-315 nm and probed the products with Fourier transform infrared spectroscopy. The strong Hbond in the enolone significantly broadens and red-shifts the OH stretch and also red-shifts the C=O stretch, relative to the free OH and C=O vibrations. After photolysis, the authors observed a free OH stretch in the 3550-3620 cm<sup>-1</sup> region and a blue-shifted C=O stretch. These results are consistent with photoinduced rotation of the OH group and breaking of the hydrogen bond, forming a higher-energy enolone conformer that is stabilized in the Xe matrix. They concluded that this is the only process resulting from the S<sub>2</sub> ( $\pi\pi^*$ ) excitation, and specifically that phototautomerization to the diketone does not occur. In later studies on UV irradiation of matrix-isolated AcAc, Nagashima et al.<sup>17</sup> detected different rotational isomers of the enolone, presumably formed by excited-state rotation about C—C bonds in the enolone. Unlike Roubin, Nagashima reported phototautomerization to the diketone; however, they saw no dissociation products. Trivella et al. 19 observed UVinduced formation of four new isomers (from 180° rotations about the  $C_3$ — $C_4$ ,  $C_2$ — $C_3$ , and  $C_2$ —O bonds) as the main process in N2, Ne, Ar, and Xe matrixes. When O2 was doped into the matrix, they observed significant CO production, which they attributed to Norrish Type I processes (formation of  $CH_3$  or  $CH_3CO)$ , followed by reaction with  $O_2$ . Lozada-Garcia et al.  $^{16,20}$  studied the photochemistry of AcAc in para-H<sub>2</sub> matrixes and found that breaking of the H-bond and phototautomerization are the only significant channels resulting from UV excitation.

The first gas-phase study of AcAc photochemistry by Yoon et al.<sup>22,23</sup> detected OH X(<sup>2</sup>Π) products by laser-induced fluorescence (LIF) after  $(S_2 \leftarrow S_0)$  excitation and measured the OH yield as a function of photodissociation wavelength from 280-310 nm. The OH rotational-state distribution was relatively cold, peaking at N = 3-4. On the basis of a photolysis energy of 96.1 kcal·mol<sup>-1</sup> (297.5 nm) and the highest rotational energy of OH measured (5.8 kcal·mol<sup>-1</sup>),

they concluded an upper limit for the C-OH bond dissociation energy in enolone-AcAc of 90.3 kcal·mol<sup>-1</sup>. Later, Upadhyaya et al.<sup>21</sup> excited AcAc at 266, 248, and 193 nm and reported no fluorescence yield from AcAc itself, implying that it must decay only by nonradiative pathways. Like Yoon, they detected OH by LIF and noted that it forms only in the v = 0 state. They measured the center-of-mass translational energy release of 16.0 and 17.3 kcal·mol<sup>-1</sup> (266 and 248 nm excitation) for OH recoiling from a presumed CH<sub>3</sub>C(O)CHCCH<sub>3</sub> cofragment, concluding that there must be an exit barrier for OH release. They used unfocused pump and probe laser beams, stating that the OH LIF was a linear function of the intensity of both lasers. On the basis of CIS calculations of the ground and excited electronic states with small basis sets, they concluded that the OH fragmentation must occur on the lowest triplet state, which they assigned as  $^{3}(\pi\pi^{*})$ . Finally, they concluded that their interpretation of the OH formation route and their measured translational energy release were consistent with the C-OH bond strength of 90.3 kcal·mol<sup>-1</sup> proposed by Yoon.

In 2004 Xu and Zewail<sup>25</sup> used a 140 fs 266 nm pump pulse to excite gas-phase AcAc, and a 2 ps burst of 30 keV electrons to probe the ensuing dynamics by time-resolved ultrafast electron diffraction. They compared their experimental signals with predicted molecular scattering curves of plausible fragment structures. They concluded that CH3 or CH3CO loss could not explain the observed electron scattering, and that only CH<sub>3</sub>C(O)CHCCH<sub>3</sub> (the cofragment of C-OH bond cleavage in the enolone) reproduced their data. They state that "OH is the dominant channel after 266 nm excitation" and that after ultrafast  $S_2 \rightarrow S_1$  internal conversion, the rate-limiting step of OH production is  $S_1 \to T_1 \; \text{ISC}$  with a time constant of 247  $\pm$  34 ps. In 2006 Chen et al.<sup>28</sup> used complete active space self-consistent field (CASSCF) and density functional theory calculations in a theoretical study of the enolone-AcAc system. They concluded that the  $S_2 \rightarrow S_1 \rightarrow$  $T_1 \rightarrow OH + CH_3C(O)CHCCH_3$  pathway is active, supporting the results of Xu and Zewail, and that phototautomerization from enolone to diketone does not occur in the gas phase. Using a CAS(10,8) calculation with zero-point energy correction, they calculated a C-OH bond strength of 89.8 kcal·mol<sup>-1</sup>, in remarkable agreement with the experimental determination of Yoon.

Poisson et al. 26 performed the second ultrafast pump—probe study of AcAc in 2008, using 266 nm pump and 800 nm probe (multiphoton ionization) lasers. They detected cations by TOF mass spectrometry and electrons by velocity map imaging. They reported that the molecular wavepacket on the S2 state moves away from the Franck-Condon region within 70 fs, transfers to S<sub>1</sub> in 1.4 ps, and requires more than 80 ps for ISC to  $T_1$ , in rough agreement with the  $S_1 \rightarrow T_1$  time scale of Xu and Zewail.

Very recently, two more ultrafast pump-probe studies on enolone-AcAc appeared. First, Bhattacherjee et al<sup>27</sup> used <70 fs, 150 GW·cm<sup>-2</sup>, 266 nm pump pulses to excite the  $(S_2 \leftarrow S_0)$ transition and <60 fs, 280-290 eV soft X-ray pulses to probe the dynamics by near-edge X-ray absorption fine structure (NEXAFS). This probe method promotes C(1s) electrons to unoccupied valence orbitals and observes the transient change in X-ray absorption as a function of time delay from the excitation pulse. Although they could not distinguish the signature of the S<sub>2</sub> state from the S<sub>1</sub> state, they proposed that  $S_2 \rightarrow S_1$  internal conversion (IC) happens on a sub-100 fs time scale, in agreement with previous ultrafast studies. However, with a clear NEXAFS signature of  $T_1$  population, they measured the time constant for  $S_{2,1} \rightarrow T_1$  ISC as  $1.5 \pm 0.2$  ps, 2 orders of magnitude faster than the interpretations of Xu and Zewail<sup>25</sup> and Poisson et al.<sup>26</sup>

The second recent ultrafast study of enolone-AcAc by Squibb et al.<sup>24</sup> used 120-170 fs 261 nm pump pulses and 100 fs 19.23 eV probe pulses from the FERMI free electron laser to observe ion yield and photoelectron spectra (although not in coincidence). They detected ions at the m/z ratios of AcAc<sup>+</sup>,  $OH^+$ , and  $CH_x^+$  (x = 0-3) and photoelectrons, which they attributed only to the ionization of AcAc. They determined an excited-state relaxation pathway  $S_2(\pi\pi^*) \rightarrow S_1(n\pi^*) \rightarrow T_2$  $(n\pi^*) \rightarrow T_1 (\pi\pi^*)$  and drew several additional conclusions: (1) enolone to diketone phototautomerization does not occur; (2) OH fragments are generated from the vibrationally hot S<sub>0</sub> state, accessed either by IC from  $S_1$  or by ISC from  $T_1$ ; (3) on the basis of CASSCF and CASPT2 calculations, both OH and  $CH_3$  may be formed on  $S_0$  "with barriers of 4.02 and 3.67 eV, respectively"; and (4) the system "undergoes roaming dynamics on the flat portion of the  $T_1$  ( $\pi\pi^*$ ) surface." Unfortunately, the only time scale they correlated with a pathway from their time-resolved photoelectron spectra was the decay of the S2 state, which "disappears at about 50 fs

4.2. Photochemistry of Molecules with Moieties Present in Enolone-AcAc. Of the four classes of molecules that share common functional groups with AcAc, the photochemistry and dynamics of carbonyls, alkenes, and polyenes have been well studied, whereas those of enols have not. Acetaldehyde (CH<sub>3</sub>CHO) and acetone (CH<sub>3</sub>C(O)CH<sub>3</sub>) are good representatives of the carbonyls. Their lowest spinallowed transitions ( $S_1 \leftarrow S_0$ ) begin near  $\lambda = 330$  nm, peak between 275 and 290 nm, are weak ( $\sim$ 5  $\times$  10<sup>-20</sup> cm<sup>2</sup>· molecule<sup>-1</sup>), and have  $\pi^* \leftarrow$  n character, owing to the promotion of a nonbonding electron on the O atom to the  $\pi^*$ orbital of the C=O group. Some fluorescence is observable at the red edge of these bands, but photodynamics are dominated by ISC to the lowest triplet state  $T_1$   $^3(n\pi^*)$  and internal conversion to S<sub>0</sub>. By contrast, the lowest spin-allowed transitions in alkenes, e.g., ethene (C2H4) and propene  $(C_3H_6)$ , are ~1000 times stronger (~5 ×  $10^{-17}$  cm<sup>2</sup>· molecule<sup>-1</sup>) than in carbonyls. Their onsets are in the vacuum UV near  $\lambda$  = 190 nm and were traditionally classified as  $\pi^* \leftarrow$  $\pi$ , <sup>72</sup> although recent work <sup>73</sup> assigns this onset to the somewhat weaker 3s  $\leftarrow \pi$  Rydberg transition (S<sub>1</sub>  $\leftarrow$  S<sub>0</sub>), assigning the stronger  $\pi^* \leftarrow \pi$  transition  $(S_2 \leftarrow S_0)$  to onsets of 175–180 nm. Promotion of an electron to the C=C  $\pi^*$  orbital causes torsional motion around the double bond, followed by rapid ( $\sim$ 100 fs) internal conversion to S<sub>0</sub> via two distinct conical intersections<sup>74</sup> and later by fragmentation via H or H<sub>2</sub> loss within 600 fs. 75 Triplet states appear to be unimportant in the photodynamics of at least the small alkenes. 75

The conjugated  $\pi$  orbitals in enolone-AcAc resemble those of polyenes, such as 1,3-butadiene (H<sub>2</sub>C=CH—CH=CH<sub>2</sub>) and acrolein (H<sub>2</sub>C=CH—CH=O). Compared to the cases for ethene and propene, delocalization of the  $\pi$  system in 1,3-butadiene lowers the onset energy of the S<sub>2</sub>  $\leftarrow$  S<sub>0</sub> ( $\pi\pi^*$ ) transition to  $\lambda \sim 220$  nm and increases the absorption cross section<sup>76</sup> to 1  $\times$  10<sup>-16</sup> cm<sup>2</sup>·molecule<sup>-1</sup>. As in ethene, excitation to S<sub>2</sub> induces ultrafast torsion and C–C bond elongation, with a 23 fs lifetime for internal conversion from S<sub>2</sub>  $\rightarrow$  S<sub>1</sub> and a 42 fs

lifetime for IC from  $S_1 \to S_0$ . Triplet states are again apparently not involved in the dynamics. 77,78

It is sensible to assume that photodynamics of enolone-AcAc may mirror most closely those of acrolein, and one might expect the electronic spectra of both molecules to nominally have contributions from the C=O and the C=C chromophores. Indeed, acrolein has a weak  $S_1 \leftarrow S_0$   $(n\pi^*)$ transition, with a peak cross-section of  $6 \times 10^{-20}$  cm<sup>2</sup>· molecule<sup>-1</sup> at 335 nm and a much stronger  $S_2 \leftarrow S_0 (\pi \pi^*)$  transition with a peak cross-section of 5 × 10<sup>-17</sup> cm<sup>2</sup>· molecule<sup>-1</sup> at 194 nm.<sup>78</sup> These two singlet excited states also have triplet analogs:  $T_1^{-3}(n\pi^*)$  and  $T_2^{-3}(\pi\pi^*)$ . Many groups have studied the photodissociation of acrolein starting from S<sub>1</sub> and S2, with at least five product channels suggested from S2 excitation at 193 nm. Lee et al. 78 applied femtosecond timeresolved photoelectron spectroscopy to probe the ultrafast dynamics after excitation to S2 at 209 and 200 nm. As in 1,3butadiene, they found rapid  $S_2 \rightarrow S_1$  conversion (50–200 fs) via a conical intersection, followed by a 620 fs IC from  $S_1 \rightarrow$  $S_0$ . These authors speculated that ISC from  $S_1$  to the triplet manifold would have at most minor importance. However, when acrolein is excited on the  $(S_1 \leftarrow S_0)$  transition, Jen and Chen<sup>79</sup> observed clear evidence of HCO + C<sub>2</sub>H<sub>3</sub> photoproducts formed over a small exit barrier that must be on a triplet surface.

**4.3. Keto–Enol Equilibrium.** Our values of  $K_{\rm eq}$  for the tautomerization of AcAc are presented in section 3.1 and may be used in a van't Hoff analysis to extract the enthalpy and entropy change of this reaction. We assume that  $\Delta H$  and  $\Delta S$  for this tautomerization are constant over 320–600 K and fit the van't Hoff equation

$$\ln(K_{\rm eq}) = \frac{-\Delta H}{R} \cdot \frac{1}{T} + \frac{\Delta S}{R} \tag{11}$$

to our data as shown in Figure 8, yielding  $\Delta H = 4.1 \pm 0.3$  kcal mol<sup>-1</sup> and  $\Delta S = 6.8 \pm 0.5$  cal·mol<sup>-1</sup>·K<sup>-1</sup>.

Our findings are in fair agreement with Folkendt et al.<sup>61</sup> and Nakanishi et al.<sup>12</sup> results but differ strongly from those of

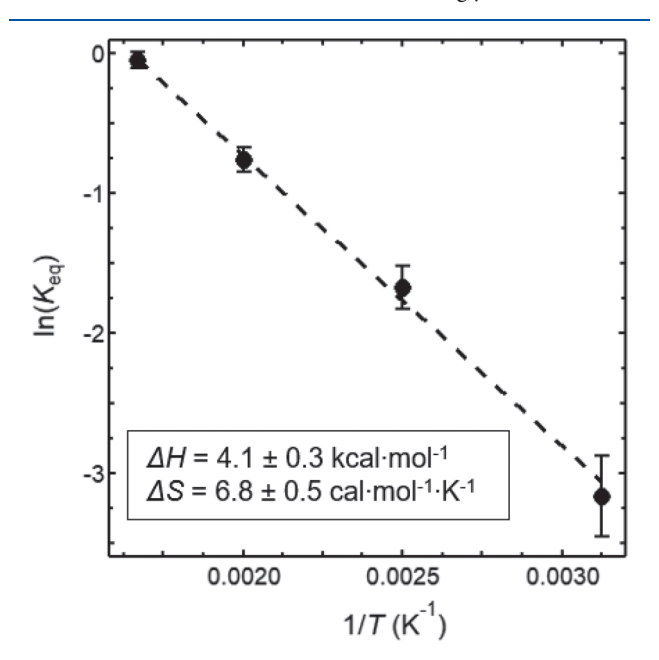


**Figure 8.** van't Hoff plot for the diketone—enolone tautomerization of AcAc, using the experimental equilibrium constants from section 3.1

Schweig et al., <sup>62</sup> as shown in Figure 1B. The work by Folkendt is a reliable point of comparison because it uses <sup>1</sup>H NMR to cleanly resolve signals, directly proportional to the enolone and diketone molar fractions. From measurements at T=373-445 K, they reported  $\Delta H=4.66\pm0.18$  kcal·mol<sup>-1</sup>, slightly outside of our determination.

Nakanishi used UV-vis spectra to measure the intensity of the strong enolone absorption feature at T = 293-477 K but could not do the same for the much weaker diketone absorption. They recognized that because  $ln(K_{eq})$  depends linearly on 1/T, by assuming a value of  $K_{eq}(293 \text{ K})$ , one can predict values of  $K_{eq}$  at other temperatures from the absorbance change of only one tautomer. Plotting  $ln(K_{eq})$  vs 1/T for a range of assumed  $K_{eq}(293 \text{ K})$ , they found curved van't Hoff plots in all cases except  $K_{eq}(293 \text{ K}) = 0.0395$  and concluded that this was the correct value at 293 K. They extracted  $\Delta H = 4.3 \text{ kcal·mol}^{-1}$  from the van't Hoff plot, in good agreement with our result. However, their  $K_{eq}(293 \text{ K})$ differs from our value of  $0.03 \pm 0.003$ , implying that their analysis would have given  $\Delta S$  (which they do not report) that conflicts with ours. This discrepancy may be due to temperature dependence of the UV-vis spectrum of enolone-AcAc. In contrast, we quantify both tautomers at each temperature and demonstrate that the PI cross section we use here does not appear to depend on T (see Figure S1).

Lastly, Schweig et al. used photoelectron spectroscopy, which did not completely resolve the enolone and diketone signals. Their analysis assumed that photoelectron spectra of diketone and enolone both consist of two peaks of equal intensity and that total ionization cross sections of the two tautomers are equal. The latter assumption is incorrect, according to our measurements (see Figure 1C), and as a result, they strongly overestimated  $K_{\rm eq}$  at all temperatures.

**4.4.** One-Photon Photochemical Pathways. Table 2 summarizes our observed primary photoproducts of enolone-AcAc at 266 and 248 nm and lists the yields of these products in the limits of pure one-photon and pure two-photon excitation, extracted from fluence-dependent data. UV excitation leads either to tautomerization of enolone to diketone or to photodissociation. On the basis of our isomer-resolved product assignments, laser fluence dependence, and quantum chemical calculations, we report six distinct one-photon product channels, as shown in Figure 7:

- I. Phototautomerization of enolone-AcAc to diketone-AcAc
- II. Methane + acetyl ketene
- III. Water + acetyl allene
- IV. Ketene +1-propen-2-ol
- V. Ketene + acetone
- VI. Acetyl + acetonyl/2-hydroxypropen-1-yl

For the dissociation pathways, we quantify both coproducts of channels IV and V, but only one product of channels II, III, and VI.

Because our experiments occur in a collisional environment, one might ask whether the species we observe are primary photoproducts or the results of chemical reactions of primary products with each other or with AcAc. The PIMS data for product identification used an initial AcAc concentration of 1.8  $\times$   $10^{12}$  molecules·cm $^{-3}$ . Assuming a worst-case scenario, in which a species such as OH reacted with a gas kinetic rate constant ( $k_{\rm GK}=10^{-10}~{\rm cm}^3{\rm \cdot molecule}^{-1}{\rm \cdot s}^{-1}$ ) with the precursor,  $^{80}$  the pseudo-first-order rate constant of this

reaction would be  $k_{\rm GK}^*[{\rm AcAc}]_0 = 180~{\rm s}^{-1}$ , implying an observed product rise time of 5.6 ms. Second-order reactions would have the same worst-case  $t_{1/2}$  times. A 5.6 ms rise time would be easily discerned by our apparatus, which has an instrument response time  $\le 0.3$  ms. All the reported products have instrument-limited rise times and therefore are primary photoproducts. In the limit of single-photon excitation, the combined yield of channels I–VI is 78% (Table 2). Considering the error bars on these yields and the universal nature of photoionization with mass spectrometric detection, there are likely no significant unobserved channels.

I. Phototautomerization of Enolone-AcAc to Diketone-AcAc. Keto—enol tautomerization in AcAc is a pericyclic H-transfer via a four-membered ring transition state TS1. Although this pathway was observed in cryogenic matrixes, <sup>17,20</sup> it was discounted in the gas-phase experiments by Xu and Zewail. <sup>25</sup> Chen et al. <sup>28</sup> calculated the S<sub>0</sub> and T<sub>1</sub> tautomerization barriers to lie 58 and 110 kcal·mol<sup>-1</sup> above the S<sub>0</sub> minimum of enolone-AcAc, respectively. Our calculated TS1 energy is close to Chen's: 59.5 kcal·mol<sup>-1</sup>. Chen et al. deemed photoinduced tautomerization to be insignificant on T<sub>1</sub> for 250 nm excitation ( $E_{h\nu} = 114.4 \text{ kcal·mol}^{-1}$ ) and did not consider it on S<sub>0</sub>.

In contrast to all previous gas-phase work, we find that phototautomerization is the most important one-photon process at either 266 or 248 nm excitation. In the limit of pure one-photon excitation, its yield is  $\Phi_{\rm I}^{(1)}$  = 29 ± 4% at 248 nm; although we did not perform fluence dependence PIMS studies with 266 nm pump pulses, qualitatively it is similarly intense at 266 nm. One-photon transitions at 248 and 266 nm provide 107.5 and 115.3 kcal·mol<sup>-1</sup> of energy to enolone-AcAc. If the calculated T<sub>1</sub> barrier height by Chen et al. is correct, then tautomerization on T<sub>1</sub> is not energetically allowed in the case of one-photon excitation at 266 nm and is also likely not favored at 248 nm. Conversely, on the electronic ground state, TS1 is isoenergetic with TS2 as the lowest energy barrier leading out of the enolone-AcAc minimum. Therefore, the calculated PES in Figure 7 suggests that if the excited enolone relaxed to  $S_0$ , phototautomerization should be a major product, in agreement with our experiments.

II. Methane + Acetyl Ketene. Our calculations found two plausible methane loss channels from enolone-AcAc. Only one of these channels, CH<sub>4</sub> + acetyl ketene, is supported by the experiments. On  $S_0$ , the calculated saddle point for this process is TS2, a six-membered ring structure, which lies 59.5 kcalmol<sup>-1</sup> above the enolone minimum and is accessible via rotation about the C<sub>3</sub>-C<sub>4</sub> bond. Matrix isolation studies have observed the stabilized product of this rotation after UV irradiation, 17 indicating that relaxation of excited enolone samples this rotated geometry. In our experiments, there is no matrix to stabilize this higher-energy isomer, and one-photon excitation provides more than enough energy to surmount TS2. The saddle point for the other  $(CH_4 + hydroxyvinyl)$ ketene) channel, TS3, requires rotation about the C<sub>3</sub>-C<sub>4</sub> and  $C_2 = C_3$  bonds and is much higher in energy, 88.4 kcal·mol<sup>-1</sup>. We also found two other transition states for CH<sub>4</sub> loss (TS9 and TS10, see the Supporting Information), but they had even higher energies of 111 and 107 kcal·mol<sup>-1</sup>, respectively, and were omitted from Figure 7 for clarity.

On the basis of our measurements alone, we cannot exclude the formation of  $CH_4$  + acetyl ketene on  $T_1$ . However, channel I is clear evidence that large portions of the excited-state population relax by converting to  $S_0$ . From the calculated

barrier heights, we expect the flux from the nascent vibrationally hot  $S_0$  population through TS2 to be similar to that through TS1, with essentially no flux through TS3. Indeed, our experimental results are consistent with this statistical dissociation picture: we observe no hydroxyvinyl ketene, but the limiting one-photon yield of  $CH_4$  + acetyl ketene,  $\Phi_{II}^{(1)}=12\pm4\%$ , is comparable to that of channel I.

III. Water + Acetyl Allene. Our calculations found two reasonable coproducts of  $H_2O$  elimination: acetyl propyne and acetyl allene, accessible on  $S_0$  from only the enolone tautomer via four-membered ring saddle points TS4 and TS5. These strained transition states involve H atom transfer to the OH moiety from the terminal  $C_1$  or the central  $C_3$  atom, respectively, with calculated energies of 88.2 and 93.3 kcal·mol<sup>-1</sup>. For  $H_2O$  + acetyl propyne, Chen et al.<sup>28</sup> reported a  $T_1$  barrier of 142 (B3LYP) or 157.7 (CASSCF) kcal·mol<sup>-1</sup> above the enolone  $S_0$  minimum, and an  $S_0$  barrier of 89.6 kcal·mol<sup>-1</sup>, in reasonable agreement with our result of 93.3 kcal·mol<sup>-1</sup> for TS5. They did not calculate either the  $T_1$  or  $S_0$  barrier for the  $H_2O$  + acetyl allene channel.

Our TPE spectrum of m/z = 82 products agrees well with the calculated spectrum of acetyl allene but shows no indication of acetyl propyne or any other coproducts. The measured yield for channel III in the limit of pure one-photon excitation is  $\Phi_{\rm III}^{(1)}$  = 25 ± 4% at 248 nm, only slightly smaller than the channel I yield and a factor of 2 larger than the yield of channel II. If H<sub>2</sub>O loss occurred on S<sub>0</sub>, this high yield would be remarkable, because the high energy and "tight" character of TS5 should render it negligible relative to TS1 and TS2. It would also be surprising that no acetyl propyne is formed, despite TS4 being ~5 kcal·mol<sup>-1</sup> lower in energy than TS5. These observations suggest that channel III is not a statistical dissociation on S<sub>0</sub> but rather occurs on an excited electronic state-mostly likely  $T_1$ , in view of the rapid 1.5  $\pm$  0.2 ps formation of T<sub>1</sub> observed by Bhattacherjee and Leone.<sup>27</sup> We note that triplet-state dissociation into nonradical products must necessarily produce a correlated (singlet + triplet) product pair. Due to the high (~7 eV) triplet-state energy of H<sub>2</sub>O<sub>1</sub><sup>81</sup> the products in our case would be singlet water + triplet acetyl allene, yet the acetyl allene products we detect are in their singlet ground state. This implies that either (1) the dynamics of channel III are governed by the evolution on T<sub>1</sub> but access S<sub>0</sub> prior to complete dissociation or (2) channel III occurs entirely on T<sub>1</sub> but acetyl allene is quenched to its ground electronic state before being detected in our experiments.

IV. Ketene + 1-Propen-2-ol. V. Ketene + Acetone. To quantify channel IV, we first measured the absolute photoionization cross section of 1-propen-2-ol, produced from 248 nm induced Norrish Type II fission of 2-pentanone<sup>82</sup> (see Supporting Information). In doing so we observed no reversion of 1-propen-2-ol to its more stable tautomer, acetone, in the same quartz reactor employed for the AcAc experiments. Therefore, we interpret the production of 1propen-2-ol and acetone as separate product channels, each with ketene as the coproduct. On S<sub>0</sub> 1-propen-2-ol may be formed from either enolone (TS6) or diketone (TS7), but acetone can only plausibly arise from diketone (TS8). TS6 and TS8 are strained four-membered ring structures, in which H atom transfers from the terminal to the central C atom, resulting in high calculated energies of 84.2 and 89.9 kcalmol<sup>-1</sup>, respectively. TS7 has a more relaxed six-membered ring geometry involving rotation about the C<sub>3</sub>-C<sub>4</sub> bond and H

transfer from  $C_5$  to an O atom, with a calculated energy of 57.4 kcal·mol $^{-1}$ .

On the basis of the measured fluence dependence of 1-propen-2-ol and acetone, we derive one-photon limiting yields  $\Phi_{\rm IV}^{(1)}=3.7\pm1.6\%$  and  $\Phi_{\rm V}^{(1)}=3\pm1.4\%$ , respectively. Because phototautomerization (channel I) occurs most likely on  $S_0$  with high yield, it is plausible that some of the nascent diketone-AcAc contains sufficient vibrational energy to go over TS6, TS7, and TS8. However, it is not clear why channel IV, which has the lowest barrier (TS7), does not dominate over channel V. All three products (ketene, acetone, and 1-propen-2-ol) are formed via both one-photon and two-photon processes (Table 2), making it more difficult to extract accurate yields. The fitted one-photon yield of ketene  $(2^{+4}_{-2}\%)$  is rather uncertain but is consistent with the sum of one-photon yields  $\Phi_{\rm II}^{(1)}+\Phi_{\rm V}^{(1)}$ , within error bars.

VI. Acetyl + Acetonyl. Acetyl + acetonyl formation is not feasible directly from the enolone. Alternatively, acetyl + 2-hydroxypropen-1-yl could be formed by C<sub>3</sub>–C<sub>4</sub> bond fission of the enolone, as shown in Figure 7. The calculated energy of these products is 109 kcal·mol<sup>-1</sup>, making them unlikely at 266 nm; yet, we see comparable acetyl signals after either 266 or 248 nm excitation. Isomerization of 2-hydroxypropen-1-yl to acetonyl has an additional barrier<sup>83</sup> of 34 kcal·mol<sup>-1</sup>, making this two-step route to acetyl + acetonyl energetically prohibited from enolone-AcAc. However, acetyl + acetonyl are logical coproducts of simple barrierless Norrish type I bond fission from the diketone, which is formed in significant yields via channel I. Therefore, we propose that channel VI proceeds via the energized diketone-AcAc intermediate on S<sub>0</sub>, similarly to channels IV and V.

Although we cannot quantify acetonyl, we recently measured the absolute PI cross-section of acetyl; it is summarized in the Supporting Information and will be reported in detail in a future publication. From the acetyl signals, we report the one-photon limiting yield  $\Phi_{\rm VI}^{(1)}=5\pm4\%$ . The calculated asymptotic energy of acetyl + acetonyl is 76.7 kcal·mol $^{-1}$ —greater than TS7, yet smaller than TS6 and TS8. Furthermore, channel VI should have an entropically favored loose transition state. As a result, it is quite plausible that it could compete with the tight transition state of TS7.

**4.5. Two-Photon Photochemical Pathways.** As established by Figure 6, methyl, hydroxyl, propargyl, allene, propyne, and ketene arise from two-photon absorption by enolone-AcAc. Although it is beyond our present scope to explore the detailed pathways of two-photon products, we note that they are reasonable from an energetic and mechanistic standpoint. The highest-energy channel that we calculated (CH<sub>3</sub> + OH + CO + propyne; see Figure 7 and Table S2) requires 150.1 kcal·mol<sup>-1</sup> of energy and forms three of the most abundant two-photon products that we observe. It is accessible by two-photon excitation at 266 or 248 nm, which supply 215 or 231 kcal·mol<sup>-1</sup> of energy, respectively, and leave 65 or 81 kcal·mol<sup>-1</sup> for product translational and internal energies.

The large absorption cross section of the  $(\pi\pi^*)$   $(S_2 \leftarrow S_0)$  transition in enolone-AcAc makes it very easy to partially saturate this transition. Therefore, we cannot rule out that three-photon excitations or sequential multiphoton processes (i.e., primary products absorbing another photon) contribute to the products we assign as two-photon. We also note that the total atom balance in the limit of pure two-photon excitation (i.e., the sum of  $\Phi_i^{(2)}$  in Table 2) falls far short of 100%. This

suggests that many multiphoton products were not detected in our experiments, perhaps because they are very short-lived radical species.

4.6. Comparison with Previous Work. Until now, OH formation was accepted as the dominant one-photon product of AcAc excitation, and earlier experimental<sup>21,22</sup> and theoretical<sup>28</sup> determinations of the C-OH bond energy in enolone-AcAc are tightly clustered in agreement at ~90 kcal· mol<sup>-1</sup>. Yet, this is unreasonably low for an enolic molecule with an internal hydrogen bond. First, the C atom bonded to OH in enolone-AcAc is formally sp<sup>2</sup>-hybridized, strengthening the C-OH bond vs an sp<sup>3</sup>-hybridized carbon. Highly accurate C-OH bond strengths from Active Thermochemical Tables  $(ATcT)^{84}$  are 92.04  $\pm$  0.03 kcal·mol<sup>-1</sup> for ethanol (an sp<sup>3</sup> carbon) and 107.8  $\pm$  0.2, i.e. ~16 kcal·mol<sup>-1</sup> higher, for ethenol (an sp<sup>2</sup> carbon). Second, an unusually strong hydrogen bond of 12.5 kcal·mol<sup>-1</sup> must be broken to remove the OH from enolone-AcAc. 11 A group additivity estimate for the OH dissociation energy is the sum of the enolic C-OH bond (e.g., in ethenol) and the H-bond energies, or around 120 kcalmol<sup>-1</sup>. Our CBS-QB3 calculations predict a 121.7 kcal·mol<sup>-1</sup> C-OH bond strength in enolone, close to the group additivity estimate. The CBS-QB3 method has a mean absolute error of 0.9 kcal·mol<sup>-1</sup> and a maximum error of 2.8 kcal·mol<sup>-1</sup> for the G2 test set of molecules.<sup>55</sup> For comparison, the CBS-QB3 calculated C-OH bond energy in ethenol is 107.55 kcal·mol<sup>-1</sup>, in excellent agreement with ATcT. Considering (1) these accurately known bond strengths, (2) our CBS-QB3 calculations on enolone-AcAc, and (3) our clear two-photon fluence dependence of OH production, it is essentially impossible that the literature C-OH bond energy of ~90 kcal·mol<sup>-1</sup> in enolone-AcAc is correct.

Recognizing that the photochemistry of enolone-AcAc is much richer than previously appreciated, what can we say about how the different functional groups in this molecule influence its photochemistry? The extremely strong ( $S_2 \leftarrow S_0$ ) transition in enolone-AcAc, compared to the weak near-UV absorptions in carbonyl molecules, indicates that the ( $\pi\pi^*$ ) transition arises mostly from the C=C  $\pi$  bond as in alkenes. However, electron delocalization in the  $\pi$  system, enabled by the conjugated O=C-C=C backbone (as in polyenes), redshifts the enolone transition, compared to the case for alkenes. This red shift is larger in enolone-AcAc than in acrolein, consistent with increased electron delocalization from the proposed aromatic character of the six-membered ring in the enolone suggested by Dannenberg and Rios. 11

Previous studies of alkenes and polyenes have observed dissociation time scales <1 ps. 85 The proposed ultrafast relaxation pathways in these systems generally invoke conical intersections among S2, S1, and S0; triplet states appear to be unimportant.<sup>77</sup> By contrast, the photochemical pathways of carbonyls are dominated by ISC to triplet states, 86 although ultrafast studies of enones do not invoke triplet states.<sup>78</sup> In enolone-AcAc, all the ultrafast experimental studies invoke ISC from the initially excited  $S_2$   $(\pi\pi^*)$  state, generally via an  $S_1$  $(n\pi^*)$  intermediate, to the  $T_2$   $(n\pi^*)$  or  $T_1$   $(\pi\pi^*)$  states. In this sense, enolone-AcAc appears to absorb near-UV light on the basis of its polyene character but decay via triplet-state pathways reminiscent of carbonyl molecules. However, all the ultrafast studies of enolone-AcAc utilize high laser fluences and are almost certainly affected by multiphoton excitation processes. Hence there is a need for ultrafast studies that can be clearly associated with single photon excitation.

The best evidence for ISC to triplet states in enolone-AcAc comes from the work of Bhattacherjee and Leone, 27 who obtained a rather clean correspondence between experimental and theoretical soft X-ray absorption signatures of population transfer to the  $T_1$  ( $\pi\pi^*$ ) state 1.5  $\pm$  0.2 ps after 266 nm excitation. As they point out, El-Sayed's rules<sup>87</sup> for ISC require that allowed (i.e., strong) couplings include a change of both orbital and spin angular momentum. Hence transfer from S<sub>1</sub>  $(n\pi^*)$  to  $T_1(\pi\pi^*)$  is allowed, but  $S_1(n\pi^*)$  to  $T_2(n\pi^*)$  is not. Because the spin-allowed nature of internal conversion from S<sub>2</sub> to S<sub>1</sub> will likely make it the fastest coupling in this system, there is both experimental and theoretical evidence to support the ultrafast conversion pathway of  $S_2$   $(\pi\pi^*) \rightarrow S_1$   $(n\pi^*) \rightarrow T_1$  $(\pi\pi^*)$ . Xu and Zewail<sup>25</sup> assign their electron scattering signal with a 247  $\pm$  34 ps formation time scale to the coproduct of OH elimination,  $CH_3CCHC(O)CH_3$ , in its  $T_1$  ( $\pi\pi^*$ ) state. However, this is likely incorrect because the CH3CCHC(O)CH3 radical would have too much internal energy to survive. Using the same excitation as Xu and Zewail (266 nm), Upadhyaya et al.<sup>21</sup> measured the translational energy release of 16.0 kcal mol<sup>-1</sup> for OH production, along with rotational energy of 1.9 kcal·mol<sup>-1</sup> and no vibrational excitation of OH. Given that this is in fact a two-photon channel, the presumed OH coproduct would have 215 - 121.7 $-16 - 1.9 = 75.4 \text{ kcal·mol}^{-1}$  of average internal energy, making it unlikely to persist and be experimentally detected for hundreds of picoseconds. Similarly, the 1.4 ps time constant in the ultrafast photoelectron spectroscopy study by Poisson et al. 26 likely represents the  $S_1$   $(n\pi^*) \rightarrow T_1$   $(\pi\pi^*)$  transfer observed by Bhattacherjee and Leone, not the  $S_2(\pi\pi^*) \rightarrow S_1$  $(n\pi^*)$  coupling they invoked.

The most recent ultrafast study by Squibb et al. <sup>24</sup> reports a 50 fs disappearance time scale of the  $S_2$  state, despite the fact that this value is significantly shorter than their convolved pump and probe pulse widths. Their choice of 19.23 eV probe photons causes significant dissociative ionization in the probe step, as evidenced by their observation of  $CH_2^+$ ,  $CH^+$ , and  $C^+$ . They claim that these fragment ions all arise from neutral  $CH_3$  radicals, and yet the time traces of these ions are all different from the time trace of  $CH_3^+$ . It is therefore not credible that these signals represent  $CH_3$  formation, raising questions about their interpretation of this product channel. Finally, their assignment of roaming dynamics on the  $T_1$  ( $\pi\pi^*$ ) surface appears to be based solely on the existence of a flat region on this surface, rather than any experimental evidence. We therefore view this conclusion as unproven.

Although our experiments do not provide direct proof of a further ISC step transferring population from  $T_1$  ( $\pi\pi^*$ ) to the  $S_0$  state, it appears probable that channel I (possibly along with II and IV–VI) occur on  $S_0$ . However, the time scale for this process is unclear. Similar  $T_1 \to S_0$  dynamics are unambiguously documented in carbonyl molecules. <sup>86</sup> Unfortunately, there is not much to say about the effect of the enol functional group on the photochemistry of enolone-AcAc due to the lack of studies on the gas-phase UV photochemistry of enols, likely because most enols are difficult to produce.

### 5. CONCLUSION

We have used three complementary techniques to study the photochemistry of the enolone tautomer of acetylacetone, excited at 266 and 248 nm using nanosecond pulsed lasers. In contrast to previous work, the universal nature of PIMS and PEPICO reveals much richer photochemistry than was

previously appreciated. We show conclusively that both oneand two-photon processes are possible after exciting the strong ( $S_2 \leftarrow S_0$ ) transition in enolone-AcAc. Our experiments and calculations indicate that the main product channel reported in the literature, OH + CH<sub>3</sub>CCHC(O)CH<sub>3</sub>, is in fact only possible via two-photon absorption at these wavelengths. The large amount of energy deposited by two-photon excitation makes it unlikely that the purported OH coproduct survives intact. Consequently, conclusions of the previous product studies in this system are largely invalid, including the 90 kcalmol<sup>-1</sup> C–OH bond strength in enolone-AcAc that was, until now, supported by both theory and experiment. Our calculated C–OH bond strength is 121.7 kcal-mol<sup>-1</sup>.

We demonstrate that phototautomerization to the diketone is a major process in the gas phase (at least at  $1-10~\rm Torr$ ) and propose that it is an intermediate on the way to other bimolecular products. We measure the enolone: diketone equilibrium constant as a function of temperature and extract  $\Delta H = 4.1 \pm 0.3~\rm kcal~mol^{-1}$  and  $\Delta S = 6.8 \pm 0.5~\rm cal\cdot mol^{-1} \cdot K^{-1}$  for this process. We quantify both one- and two-photon product channels but caution the reader that the ratios of these two product groups will depend on the excitation wavelength and photon fluence.

Because acetylacetone exhibits some characteristics of enols, carbonyls, and polyenes, it a fascinating test bed for fundamental studies of light absorption by complex molecules with multiple functional groups. Our work illuminates several outstanding questions that could be answered by further studies of AcAc. Understanding the time scale for intersystem crossing from  $T_1$  ( $\pi\pi^*$ )  $\to$   $S_0$  will require ultrafast spectroscopic measurements that are sensitive to the  $S_0$  population. Furthermore, although we have some evidence regarding which one-photon products are born on  $S_0$  vs excited electronic states, dynamics experiments probing translational and product state distributions, along with high-quality calculations of excited electron states, will be required for definitive answers.

#### ASSOCIATED CONTENT

#### **S** Supporting Information

The Supporting Information is available free of charge on the ACS Publications website at DOI: 10.1021/acs.jpca.9b04640.

Temperature-dependent PI spectra of daughter ions of acetylacetone; details of photoproduct identification; typical time traces of photoproducts; absolute PI cross-section measurements of reference compounds; assignment of daughter ions of the acetonyl radical; calculations of the neutral and cation PES of diketone-AcAc; calculations of stationary points and energy barriers on the  $S_0$  PES of acetylacetone and of dissociation products (PDF)

#### AUTHOR INFORMATION

#### **Corresponding Author**

\*E-mail: lsheps@sandia.gov.

ORCID ®

Krisztina Voronova: 0000-0003-2252-9143 Bálint Sztáray: 0000-0002-0333-0000 Patrick Hemberger: 0000-0002-1251-4549 Andras Bodi: 0000-0003-2742-1051 Leonid Sheps: 0000-0003-4320-0865

#### **Present Addresses**

Department of Chemistry, University of Nevada, Reno, NV 89557, USA.

<sup>1</sup>KLA-Tencor Corp., Milpitas, CA 95035, USA.

#### Notes

The authors declare no competing financial interest.

#### ACKNOWLEDGMENTS

The PEPICO experiments were carried out at the Swiss Light Source (Paul Scherrer Institute, Villigen, Switzerland). P.H. and A.B. gratefully acknowledge funding by the Swiss Federal Office of Energy (BFE Contract Number SI/501269-01). B.Sz. and K.V. gratefully acknowledge funding by the National Science Foundation (Grant No. CHE-1665464). The contributions of D.L.O. and M.W.C. and the development of all three experimental apparatuses are based upon work supported by the Office of Chemical Sciences, Geosciences, and Biosciences, Office of Basic Energy Sciences, United States Department of Energy. L.S. and I.A. were supported by the Division of Chemical Sciences, Geosciences and Biosciences, BES/USDOE, through the Argonne-Sandia Consortium on High Pressure Combustion Chemistry. Sandia National Laboratories is a multimission laboratory managed and operated by National Technology and Engineering Solutions of Sandia, LLC., a wholly owned subsidiary of Honeywell International, Inc., for the USDOE's National Nuclear Security Administration under contract DE-NA0003525. The Advanced Light Source is supported by the Director, Office of Science, Office of Basic Energy Sciences, of the U.S. Department of Energy under Contract No. DE-AC02-05CH11231. The views expressed in the article do not necessarily represent the views of the U.S. Department of Energy or the United States Government.

#### REFERENCES

- (1) Schoenlein, R. W.; Peteanu, L. A.; Mathies, R. A.; Shank, C. V. The 1st step in vision femtosecond isomerization of rhodopsin. *Science* **1991**, 254, 412–415.
- (2) Polli, D.; Altoe, P.; Weingart, O.; Spillane, K. M.; Manzoni, C.; Brida, D.; Tomasello, G.; Orlandi, G.; Kukura, P.; Mathies, R. A.; et al. Conical intersection dynamics of the primary photoisomerization event in vision. *Nature* **2010**, *467*, 440–443.
- (3) Romonosky, D. E.; Li, Y.; Shiraiwa, M.; Laskin, A.; Laskin, J.; Nizkorodov, S. A. Aqueous photochemistry of secondary organic aerosol of alpha-pinene and alpha-humulene oxidized with ozone, hydroxyl radical, and nitrate radical. *J. Phys. Chem. A* **2017**, *121*, 1298–1309.
- (4) Kawaguchi, S. Variety in the coordination modes of betadicarbonyl compounds in metal-complexes. *Coord. Chem. Rev.* **1986**, 70, 51–84.
- (5) Thornton, D. A. Infrared-spectra of metal beta-ketoenolates and related complexes. *Coord. Chem. Rev.* **1990**, *104*, 173–249.
- (6) Nematollahi, D.; Rafiee, M. Diversity in electrochemical oxidation of dihydroxybenzoic acids in the presence of acetylacetone. A green method for synthesis of new benzofuran derivatives. *Green Chem.* **2005**, *7*, 638–644.
- (7) Zhang, S. J.; Liu, X. T.; Wang, M. S.; Wu, B. D.; Pan, B. C.; Yang, H.; Yu, H. Q. Diketone-mediated photochemical processes for target-selective degradation of dye pollutants. *Environ. Sci. Technol. Lett.* **2014**, *1*, 167–171.
- (8) Meyer, K. H. The connection between the constitution and equilibrium of keto-enol-desmotropic compounds (Keto-enol-tautomerism VI). *Ber. Dtsch. Chem. Ges.* **1912**, *45*, 2843–2864.

- (9) Conant, J. B.; Thompson, A. F. The free energy of enolization in the gaseous phase of substituted acetoacetic esters. *J. Am. Chem. Soc.* **1932**, *54*, 4039–4047.
- (10) Powling, J.; Bernstein, H. J. The effect of solvents on tautomeric equilibria. J. Am. Chem. Soc. 1951, 73, 4353–4356.
- (11) Dannenberg, J. J.; Rios, R. Theoretical-study of the enolic forms of acetylacetone how strong is the H-bond. *J. Phys. Chem.* **1994**, *98*, 6714–6718.
- (12) Nakanishi, H.; Morita, H.; Nagakura, S. Electronic-structures and spectra of keto and enol forms of acetylacetone. *Bull. Chem. Soc. Jpn.* 1977, 50, 2255–2261.
- (13) Grossmann, P. The tautomery of acetoacetic acid and the acatylacetones. The absorbtion spectrum of these and related compounds. Z. Phys. Chem. 1924, 109, 305–352.
- (14) Messaadia, L.; El Dib, G.; Ferhati, A.; Chakir, A. UV-visible spectra and gas-phase rate coefficients for the reaction of 2,3-pentanedione and 2,4-pentanedione with OH radicals. *Chem. Phys. Lett.* **2015**, *626*, 73–79.
- (15) Walzl, K. N.; Xavier, I. M.; Kuppermann, A. Electron-impact spectroscopy of various diketone compounds. *J. Chem. Phys.* **1987**, *86*, 6701–6706.
- (16) Lozada-Garcia, R. R.; Ceponkus, J.; Chevalier, M.; Chin, W.; Mestdagh, J. M.; Crepin, C. Photochemistry of acetylacetone isolated in parahydrogen matrices upon 266 nm irradiation. *Phys. Chem. Chem. Phys.* **2012**, *14*, 3450–3459.
- (17) Nagashima, N.; Kudoh, S.; Takayanagi, M.; Nakata, M. UV-induced photoisomerization of acetylacetone and identification of less-stable isomers by low-temperature matrix-isolation infrared spectroscopy and density functional theory calculation. *J. Phys. Chem. A* **2001**, *105*, 10832–10838.
- (18) Roubin, P.; Chiavassa, T.; Verlaque, P.; Pizzala, L.; Bodot, H. FTIR study of UV-induced isomerization of intramolecularly hydrogen-bonded carbonyl compounds isolated in xenon matrices. *Chem. Phys. Lett.* **1990**, *175*, 655–659.
- (19) Trivella, A.; Wassermann, T. N.; Mestdagh, J. M.; Tanner, C. M.; Marinelli, F.; Roubin, P.; Coussan, S. New insights into the photodynamics of acetylacetone: isomerization and fragmentation in low-temperature matrixes. *Phys. Chem. Chem. Phys.* **2010**, *12*, 8300–8310.
- (20) Lozada-Garcia, R. R.; Ceponkus, J.; Chin, W.; Chevalier, M.; Crepin, C. Acetylacetone in hydrogen solids: IR signatures of the enol and keto tautomers and UV induced tautomerization. *Chem. Phys. Lett.* **2011**, *504*, 142–147.
- (21) Upadhyaya, H. P.; Kumar, A.; Naik, P. D. Photodissociation dynamics of enolic-acetylacetone at 266, 248, and 193 nm: Mechanism and nascent state product distribution of OH. *J. Chem. Phys.* **2003**, *118*, 2590–2598.
- (22) Yoon, M. C.; Choi, Y. S.; Kim, S. K. Photodissociation dynamics of acetylacetone: The OH product state distribution. *J. Chem. Phys.* **1999**, *110*, 11850–11855.
- (23) Yoon, M. C.; Choi, Y. S.; Kim, S. K. The OH production from the  $\pi$ - $\pi$ \* transition of acetylacetone. *Chem. Phys. Lett.* **1999**, 300, 207–212.
- (24) Squibb, R. J.; Sapunar, M.; Ponzi, A.; Richter, R.; Kivimaki, A.; Plekan, O.; Finetti, P.; Sisourat, N.; Zhaunerchyk, V.; Marchenko, T.; et al. Acetylacetone photodynamics at a seeded free-electron laser. *Nat. Commun.* **2018**, *9*, 63.
- (25) Xu, S. J.; Park, S. T.; Feenstra, J. S.; Srinivasan, R.; Zewail, A. H. Ultrafast electron diffraction: Structural dynamics of the elimination reaction of acetylacetone. *J. Phys. Chem. A* **2004**, *108*, 6650–6655.
- (26) Poisson, L.; Roubin, P.; Coussan, S.; Soep, B.; Mestdagh, J. M. Ultrafast dynamics of acetylacetone (2,4-pentanedione) in the  $S_2$  state. *J. Am. Chem. Soc.* **2008**, 130, 2974–2983.
- (27) Bhattacherjee, A.; Das Pennaraju, C.; Schnorr, K.; Attar, A. R.; Leone, S. R. Ultrafast intersystem crossing in acetylacetone via femtosecond X-ray transient absorption at the carbon K-edge. *J. Am. Chem. Soc.* **2017**, *139*, 16576–16583.
- (28) Chen, X. B.; Fang, W. H.; Phillips, D. L. Theoretical studies of the photochemical dynamics of acetylacetone: Isomerzation, dis-

- sociation, and dehydration reactions. J. Phys. Chem. A 2006, 110, 4434-4441.
- (29) Townsend, D.; Lahankar, S. A.; Lee, S. K.; Chambreau, S. D.; Suits, A. G.; Zhang, X.; Rheinecker, J.; Harding, L. B.; Bowman, J. M. The roaming atom: Straying from the reaction path in formaldehyde decomposition. *Science* **2004**, *306*, 1158–1161.
- (30) Yang, B.; Wang, J.; Cool, T. A.; Hansen, N.; Skeen, S.; Osborn, D. L. Absolute photoionization cross-sections of some combustion intermediates. *Int. J. Mass Spectrom.* **2012**, *309*, 118–128.
- (31) Welz, O.; Savee, J. D.; Eskola, A. J.; Sheps, L.; Osborn, D. L.; Taatjes, C. A. Low-temperature combustion chemistry of biofuels: pathways in the low-temperature (550–700 K) oxidation chemistry of isobutanol and tert-butanol. *Proc. Combust. Inst.* **2013**, *34*, 493–500.
- (32) Savee, J. D.; Soorkia, S.; Welz, O.; Selby, T. M.; Taatjes, C. A.; Osborn, D. L. Absolute photoionization cross-section of the propargyl radical. *J. Chem. Phys.* **2012**, *136*, 134307.
- (33) Cool, T. A.; Nakajima, K.; Mostefaoui, T. A.; Qi, F.; McIlroy, A.; Westmoreland, P. R.; Law, M. E.; Poisson, L.; Peterka, D. S.; Ahmed, M. Selective detection of isomers with photoionization mass spectrometry for studies of hydrocarbon flame chemistry. *J. Chem. Phys.* **2003**, *119*, 8356–8365.
- (34) Cool, T. A.; Wang, J.; Nakajima, K.; Taatjes, C. A.; Mcllroy, A. Photoionization cross sections for reaction intermediates in hydrocarbon combustion. *Int. J. Mass Spectrom.* **2005**, 247, 18–27.
- (35) Welz, O.; Burke, M. P.; Antonov, I. O.; Goldsmith, C. F.; Savee, J. D.; Osborn, D. L.; Taatjes, C. A.; Klippenstein, S. J.; Sheps, L. New insights into low-temperature oxidation of propane from synchrotron photoionization mass spectrometry and multi-scale informatics modeling. *J. Phys. Chem. A* **2015**, *119*, 7116–7129.
- (36) Bierkandt, T.; Hemberger, P.; Oßwald, P.; Köhler, M.; Kasper, T. Insights in m-xylene decomposition under fuel-rich conditions by imaging photoelectron photoion coincidence spectroscopy. *Proc. Combust. Inst.* **2017**, *36*, 1223–1232.
- (37) Felsmann, D.; Moshammer, K.; Krüger, J.; Lackner, A.; Brockhinke, A.; Kasper, T.; Bierkandt, T.; Akyildiz, E.; Hansen, N.; Lucassen, A.; et al. Electron ionization, photoionization and photoelectron/photoion coincidence spectroscopy in mass-spectrometric investigations of a low-pressure ethylene/oxygen flame. *Proc. Combust. Inst.* 2015, 35, 779–786.
- (38) Hemberger, P.; Custodis, V. B.; Bodi, A.; Gerber, T.; van Bokhoven, J. A. Understanding the mechanism of catalytic fast pyrolysis by unveiling reactive intermediates in heterogeneous catalysis. *Nat. Commun.* **2017**, *8*, 15946.
- (39) Hemberger, P.; Trevitt, A. J.; Ross, E.; da Silva, G. Direct observation of para-xylylene as the decomposition product of the meta-xylyl radical using vuv synchrotron radiation. *J. Phys. Chem. Lett.* **2013**, *4*, 2546–2550.
- (40) Paunović, V.; Hemberger, P.; Bodi, A.; López, N.; Pérez-Ramírez, J. Evidence of radical chemistry in catalytic methane oxybromination. *Nat. Catal.* **2018**, *1*, 363–370.
- (41) Reusch, E.; Holzmeier, F.; Constantinidis, P.; Hemberger, P.; Fischer, I. Isomer-selective generation and spectroscopic characterization of picolyl radicals. *Angew. Chem., Int. Ed.* **2017**, *56*, 8000–8003.
- (42) Schleier, D.; Constantinidis, P.; Faßheber, N.; Fischer, I.; Friedrichs, G.; Hemberger, P.; Reusch, E.; Sztáray, B.; Voronova, K. Kinetics of the a- $C_3H_5$  +  $O_2$  reaction, investigated by photoionization using synchrotron radiation. *Phys. Chem. Chem. Phys.* **2018**, 20, 10721-10731.
- (43) Steglich, M.; Custodis, V. B.; Trevitt, A. J.; daSilva, G.; Bodi, A.; Hemberger, P. Photoelectron spectrum and energetics of the metaxylylene diradical. *J. Am. Chem. Soc.* **2017**, *139*, 14348–14351.
- (44) Schleier, D.; Humeniuk, A.; Reusch, E.; Holzmeier, F.; Nunez-Reyes, D.; Alcaraz, C.; Garcia, G. A.; Loison, J.-C.; Fischer, I.; Mitric, R. Diborene: Generation and photoelectron spectroscopy of an inorganic biradical. *J. Phys. Chem. Lett.* **2018**, *9*, 5921–5925.
- (45) Osborn, D. L.; Zou, P.; Johnsen, H.; Hayden, C. C.; Taatjes, C. A.; Knyazev, V. D.; North, S. W.; Peterka, D. S.; Ahmed, M.; Leone, S. R. The multiplexed chemical kinetic photoionization mass spec-

- trometer: A new approach for isomer resolved chemical kinetics. *Rev. Sci. Instrum.* **2008**, *79*, 104103.
- (46) Welz, O.; Zádor, J.; Savee, J. D.; Sheps, L.; Osborn, D. L.; Taatjes, C. A. Low-temperature combustion chemistry of n-butanol: Principal oxidation pathways of hydroxybutyl radicals. *J. Phys. Chem. A* **2013**, *117*, 11983–12001.
- (47) Sztáray, B.; Voronova, K.; Torma, K. G.; Covert, K. J.; Bodi, A.; Hemberger, P.; Gerber, T.; Osborn, D. L. CRF-PEPICO: Double velocity map imaging photoelectron photoion coincidence spectroscopy for reaction kinetics studies. *J. Chem. Phys.* **2017**, *147*, 013944.
- (48) Johnson, M.; Bodi, A.; Schulz, L.; Gerber, T. Vacuum ultraviolet beamline at the Swiss Light Source for chemical dynamics studies. *Nucl. Instrum. Methods Phys. Res., Sect. A* **2009**, 610, 597–603.
- (49) Sztáray, B.; Baer, T. Suppression of hot electrons in threshold photoelectron photoion coincidence spectroscopy using velocity focusing optics. *Rev. Sci. Instrum.* **2003**, *74*, 3763–3768.
- (50) Chupka, W. A. Factors affecting lifetimes and resolution of Rydberg states observed in zero-electron-kinetic-energy spectroscopy. *J. Chem. Phys.* **1993**, *98*, 4520–4530.
- (51) Pilgrim, J. S.; Jennings, R. T.; Taatjes, C. A. Temperature controlled multiple pass absorption cell for gas phase chemical kinetics studies. *Rev. Sci. Instrum.* 1997, 68, 1875–1878.
- (52) Farrell, J. T.; Taatjes, C. A. Infrared frequency-modulation probing of Cl+ C<sub>3</sub>H<sub>4</sub> (allene, propyne) reactions: kinetics of HCl production from 292 to 850 K. *J. Phys. Chem. A* **1998**, *102*, 4846–4856.
- (53) Rothman, L. S.; Gordon, I. E.; Babikov, Y.; Barbe, A.; Benner, D. C.; Bernath, P. F.; Birk, M.; Bizzocchi, L.; Boudon, V.; Brown, L. R. The HITRAN2012 molecular spectroscopic database. *J. Quant. Spectrosc. Radiat. Transfer* **2013**, *130*, 4–50.
- (54) Frisch, M. J.; Trucks, G. W.; Schlegel, H. B.; Scuseria, G. E.; Robb, M. A.; Cheeseman, J. R.; Scalmani, G.; Barone, V.; Mennucci, B.; Petersson, G. A.; et al. *Gaussian 09*, Revision A.02; Gaussian, Inc.: Wallingford, CT, 2009.
- (55) Montgomery, J. A.; Frisch, M. J.; Ochterski, J. W.; Petersson, G. A. A complete basis set model chemistry. VI. Use of density functional geometries and frequencies. *J. Chem. Phys.* **1999**, *110*, 2822–2827.
- (56) Peng, C.; Bernhard Schlegel, H. Combining synchronous transit and quasi-newton methods to find transition states. *Isr. J. Chem.* **1993**, 33, 449–454.
- (57) Mozhayskiy, V. A.; Krylov, A. ezSpectrum; University of Southern California: Los Angeles, CA, 2016.
- (58) Houk, K.; Davis, L. P.; Newkome, G. R.; Duke, R.; Nauman, R. Photoelectron spectroscopy of cyclic  $\beta$ -diketones and their enolone tautomers. *J. Am. Chem. Soc.* **1973**, *95*, 8364–8371.
- (59) Briegleb, G.; Strohmeier, W. Prinzipielle kritische bemerkungen zur theorie der keto-enol-umwandlung ergebnisse neuerer messungen über keto-enol-gleichgewichte von  $\beta$ -diketonen und deren temperaturabhängigkeit im gaszustand. *Angew. Chem.* **1952**, *64*, 409–417.
- (60) Irving, R.; Wadso, I. Enthalpy of vaporization of organic compounds at 25 degrees C. S. Acetylacetone. *Acta Chem. Scand.* 1970, 24, 589–592.
- (61) Folkendt, M. M.; Weiss-Lopez, B. E.; Chauvel, J. P., Jr; True, N. S. Gas-phase proton NMR studies of keto-enol tautomerism of acetylacetone, methyl acetoacetate, and ethyl acetoacetate. *J. Phys. Chem.* 1985, 89, 3347–3352.
- (62) Schweig, A.; Vermeer, H.; Weidner, U. A photoelectron spectroscopic study of keto-enol tautomerism in acetylacetones-a new application of photoelectron spectroscopy. *Chem. Phys. Lett.* **1974**, 26, 229–233.
- (63) Katayama, D.; Huffman, R.; O'Bryan, C. Absorption and photoionization cross sections for H<sub>2</sub>O and D<sub>2</sub>O in the vacuum ultraviolet. *J. Chem. Phys.* **1973**, *59*, 4309–4319.
- (64) Wang, J.; Yang, B.; Cool, T. A.; Hansen, N.; Kasper, T. Nearthreshold absolute photoionization cross-sections of some reaction intermediates in combustion. *Int. J. Mass Spectrom.* **2008**, 269, 210–220.
- (65) Linstrom, P. J., Mallard, W. G., Eds. NIST Chemistry WebBook; NIST Standard Reference Database Number 69; National Institute of

- Standards and Technology: Gaithersburg, MD, http://webbook.nist.gov (accessed May 30, 2019).
- (66) Fogleman, E. A.; Koizumi, H.; Kercher, J. P.; Sztáray, B.; Baer, T. Heats of formation of the acetyl radical and ion obtained by threshold photoelectron photoion coincidence. *J. Phys. Chem. A* **2004**, 108, 5288–5294.
- (67) Bombach, R.; Dannacher, J.; Honegger, E.; Stadelmann, J.-P.; Neier, R. Unimolecular dissociations of excited  $C_3H_6O^+$ : A photoelectron—photoion coincidence study of cyclopropanol and allyl alcohol. *Chem. Phys.* **1983**, 82, 459–470.
- (68) Mines, G., Thompson, H. Photoelectron spectra of vinyl and allyl halides. Spectrochim. Acta, Part A 1973, 29, 1377-1383.
- (69) Gans, B.; Garcia, G. A.; Boyé-Péronne, S.; Loison, J.-C.; Douin, S.; Gaie-Levrel, F. o.; Gauyacq, D. Absolute photoionization cross section of the ethyl radical in the range 8–11.5 eV: synchrotron and vacuum ultraviolet laser measurements. *J. Phys. Chem. A* **2011**, *115*, 5387–5396.
- (70) Savee, J. D.; Welz, O.; Taatjes, C. A.; Osborn, D. L. New mechanistic insights to the  $O(^3P)$  + propene reaction from multiplexed photoionization mass spectrometry. *Phys. Chem. Chem. Phys.* **2012**, *14*, 10410–10423.
- (71) Meloni, G.; Selby, T. M.; Goulay, F.; Leone, S. R.; Osborn, D. L.; Taatjes, C. A. Photoionization of 1-alkenylperoxy and alkylperoxy radicals and a general rule for the stability of their cations. *J. Am. Chem. Soc.* **2007**, *129*, 14019–14025.
- (72) Merer, A. J.; Mulliken, R. S. Ultraviolet spectra and excited states of ethylene and its alkyl derivatives. *Chem. Rev.* **1969**, *69*, 639–656.
- (73) Snyder, P. A.; Atanasova, S.; Hansen, R. W. C. Ethylene. Experimental evidence for new assignments of electronic transitions in the  $\pi$   $\pi^*$  energy region. Absorption and magnetic circular dichroism measurements with synchrotron radiation. *J. Phys. Chem. A* **2004**, *108*, 4194–4201.
- (74) Tao, H.; Allison, T. K.; Wright, T. W.; Stooke, A. M.; Khurmi, C.; van Tilborg, J.; Liu, Y.; Falcone, R. W.; Belkacem, A.; Martinez, T. J. Ultrafast internal conversion in ethylene. I. The excited state lifetime. *J. Chem. Phys.* **2011**, *134*, 244306.
- (75) Allison, T. K.; Tao, H.; Glover, W. J.; Wright, T. W.; Stooke, A. M.; Khurmi, C.; van Tilborg, J.; Liu, Y.; Falcone, R. W.; Martinez, T. J.; et al. Ultrafast internal conversion in ethylene. II. Mechanisms and pathways for quenching and hydrogen elimination. *J. Chem. Phys.* **2012**, *136*, 124317.
- (76) Fahr, A.; Nayak, A. K. Temperature-dependent ultraviolet absorption cross-sections of 1,3-butadiene and butadiyne. *Chem. Phys.* **1994**, *189*, 725–731.
- (77) Boguslavskiy, A. E.; Schalk, O.; Gador, N.; Glover, W. J.; Mori, T.; Schultz, T.; Schuurman, M. S.; Martinez, T. J.; Stolow, A. Excited state non-adiabatic dynamics of the smallest polyene, trans 1,3-butadiene. I. Time-resolved photoelectron-photoion coincidence spectroscopy. *J. Chem. Phys.* **2018**, *148*, 164302.
- (78) Lee, A. M. D.; Coe, J. D.; Ullrich, S.; Ho, M. L.; Lee, S. J.; Cheng, B. M.; Zgierski, M. Z.; Chen, I. C.; Martinez, T. J.; Stolow, A. Substituent effects on dynamics at conical intersections:  $\alpha,\beta$ -enones. *J. Phys. Chem. A* **2007**, *111*, 11948–11960.
- (79) Jen, S. H.; Chen, I. C. Production of HCO from propenal photolyzed near 300 nm: Reaction mechanism and distribution of internal states of fragment HCO. *J. Chem. Phys.* **1999**, *111*, 8448–8453.
- (80) Holloway, A.-L.; Treacy, J.; Sidebottom, H.; Mellouki, A.; Daële, V.; Le Bras, G.; Barnes, I. Rate coefficients for the reactions of OH radicals with the keto/enol tautomers of 2,4-pentanedione and 3-methyl-2,4-pentanedione, allyl alcohol and methyl vinyl ketone using the enols and methyl nitrite as photolytic sources of OH. *J. Photochem. Photobiol., A* **2005**, *176*, 183–190.
- (81) Chutjian, A.; Hall, R. I.; Trajmar, S. Electron-impact excitation of  $H_2O$  and  $D_2O$  at various scattering angles and impact energies in the energy-loss range 4.2–12 eV. *J. Chem. Phys.* **1975**, *63*, 892–898.

- (82) Shaw, M. F.; Osborn, D. L.; Jordan, M. J. T.; Kable, S. H. Infrared spectra of gas-phase 1-and 2-propenol isomers. *J. Phys. Chem. A* **2017**, *121*, 3679–3688.
- (83) Zádor, J.; Miller, J. A. Adventures on the  $C_3H_5O$  potential energy surface: OH + propyne, OH + allene and related reactions. *Proc. Combust. Inst.* **2015**, 35, 181–188.
- (84) Ruscic, B.; Bross, D. H. Active Thermochemical Tables (ATcT) values based on ver. 1.122d of the Thermochemical Network (2018). https://ATcT.anl.gov (accessed May 30, 2019).
- (85) Coe, J. D.; Martínez, T. J. Ab initio molecular dynamics of excited-state intramolecular proton transfer around a three-state conical intersection in malonaldehyde. *J. Phys. Chem. A* **2006**, *110*, 618–630.
- (86) Heazlewood, B. R.; Rowling, S. J.; Maccarone, A. T.; Jordan, M. J. T.; Kable, S. H. Photochemical formation of HCO and  $CH_3$  on the ground  $S_0$  ( $^1A'$ ) state of  $CH_3CHO$ . *J. Chem. Phys.* **2009**, *130*, 054310.
- (87) El-Sayed, M. A. Spin-orbit coupling and radiationless processes in nitrogen heterocyclics. *J. Chem. Phys.* **1963**, *38*, 2834–2838.